JPG Journal of Petroleum Geology www.jpg.co.uk

Journal of Petroleum Geology, Vol. 42(1), January 2019, pp 37-58

HYDROCARBON POTENTIAL AND PALAEO-DEPOSITIONAL ENVIRONMENT OF LACUSTRINE SOURCE ROCKS: MIDDLE JURASSIC SHIMENGOU FORMATION, NORTHERN QAIDAM BASIN, NW CHINA

Q. T. Meng [a,b,*], A. Bechtel[c], R. F. Sachsenhofer[c], Z. J. Liu[a,b], D. Gross[c], P. C. Sun[a,b], F. Hu[a,b], L. Li[a,b], K. B Wang[a,b], C. Xu[a,b], L. L. Chen [a,b] and W. R. Zeng[a,b]

The Middle Jurassic Shimengou Formation in the Qaidam Basin, NW China, includes coals and lacustrine source rocks which locally reach oil shale quality (i.e. yielding >3.5 % oil on low-temperature distillation). In the present study, the palaeo-depositional environment and hydrocarbon potential of the 84.5 m thick Shale Member of the Shimengou Formation are investigated based on bulk geochemical parameters, organic petrographic data, biomarker analysis, and stable isotope geochemistry of 88 core samples.

The Shale Member was deposited in an anoxic freshwater lake which formed following the drowning of a precursor low-lying mire. Variations in bulk geochemical parameters allow four informal units to be identified, referred to (from the base up) as Units 1 to 4. These contain intervals of oil shale of varying thicknesses. In Unit 1, mudstones in the interval referred to as oil shale Layer 1 (true thickness [TD]: 2.06 m) are OM-rich as a result of algal blooms and photic zone anoxia, and correspond to an initial flooding event. Subsequently, productivity of aquatic organisms decreased, resulting in the deposition of organic-lean mudstones in Unit 2. Oil shale Layers 2 (TD: 2.03 m) and 3 (TD: 8.03 m) near the base of Unit 3 were deposited during maximum water depths. As with Layer 1, high productivity by algal blooms resulted in photic zone anoxia in a stratified water column. The shales in the upper part of Unit 3 are characterized by high TOC contents and a gradual increased input of terrigenous OM, and were deposited in a stable semi-deep lake. Finally, organic-lean mudstones in Unit 4 were deposited in shallow lacustrine conditions. The reconstruction of depositional environments in thick, non-marine shale-rich successions by mineralogical, petrographic and inorganic geochemical methods may be challenging as a result of the homogenous composition of component mudstones. The results of this study indicate, however, that sub-division and basin-wide correlation of such intervals can be achieved by organic geochemical analyses.

[a] College of Earth Sciences, Jilin University, 130061 Changchun, China.
[b] Key Laboratory for Oil Shale and Paragenetic Energy Minerals, Changchun, 130061, Jilin Province, China.
[c] Department Applied Geosciences and Geophysics, Montanuniversität Leoben, Peter-Tunner Str.5, A-8700 Leoben, Austria.
* Corresponding author: mengqt@jlu.edu.cn

Key words: Biomarkers, lacustrine source rocks, depositional environment, hydrocarbon potential, oil shale, alginite, Shimengou Formation, Qaidam Basin, China.

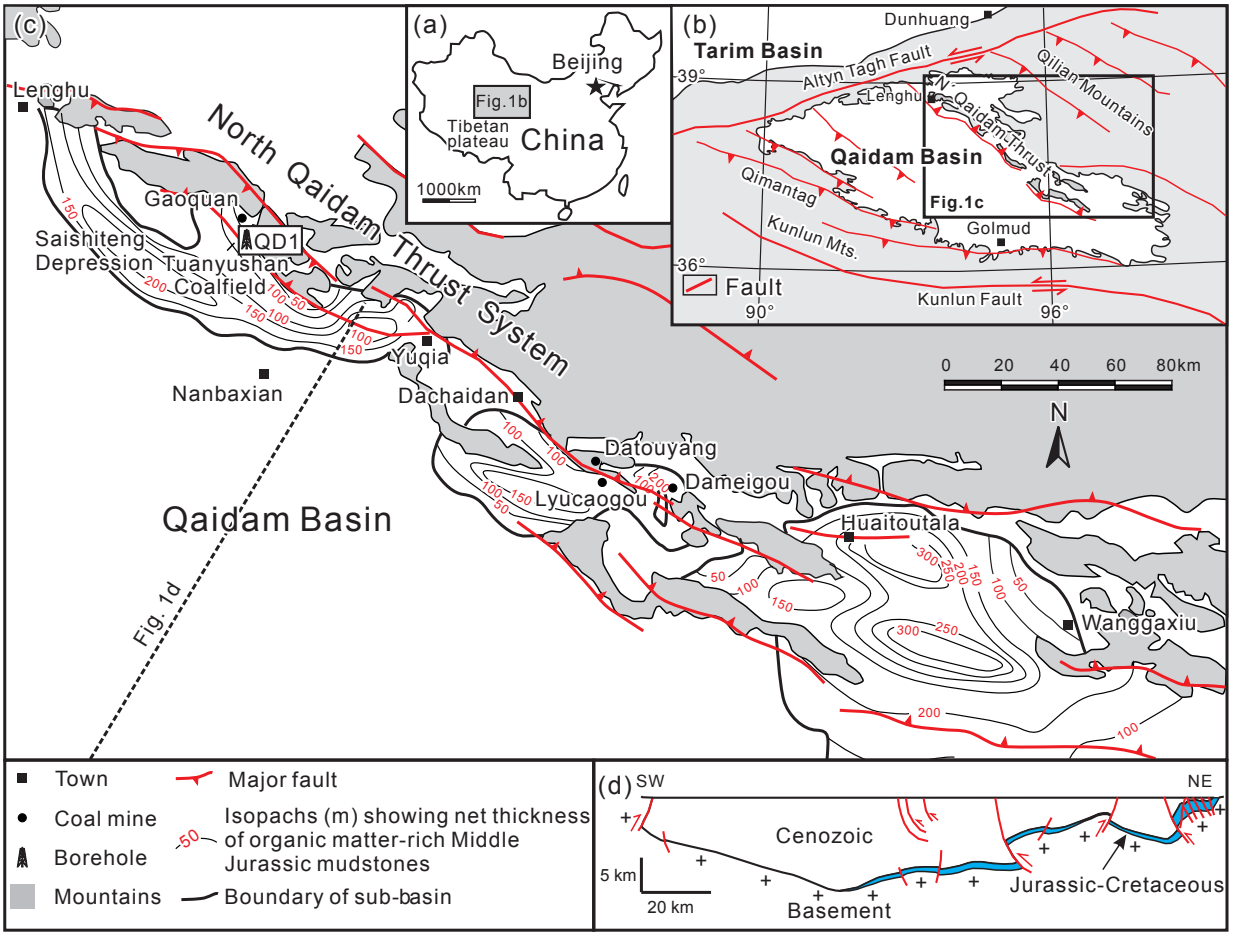

Fig. 1a. Location of the Qaidam Basin in NW China; (b) Regional-scale structures in the Qaidam Basin and surrounding area (after Dai *et al.*, 2003; Shao *et al.*, 2014); (c) Map of the study area with isopachs of OM-rich Middle Jurassic mudstones in sub-basins in the northern Qaidam Basin; also shown is the location of the QD-1 borehole (isopachs after Li, 2014); (d) cartoon SW–NE cross-section (profile line in Fig. 1c) showing the depth below surface of the Jurassic – Cretaceous interval (simplified after Bao *et al.*, 2017).

Oil shales and organic-rich mudstones in Units 1 and 3 of the Shimengou Formation Shale Member are excellent oil-prone source-rocks with a Source Potential Index of 3.2 t HC/m². Considering the large area covered by the Shimengou Formation in the northern Qaidam Basin (~34,000 km²), the results of this study highlight the regional significance for future petroleum exploration. They indicate that variations in organic productivity and dilution by minerals are key factors controlling the abundance and type of organic matter in the formation. An understanding of these factors will assist with the identification of exploration targets.

INTRODUCTION

The non-marine Qaidam Basin covers an area of about 250,000 km² and is located near the northern margin of the Tibet plateau (NW China) (Fig. 1a, b). An intracontinental rift during the Early to Middle Jurassic developed into a foreland basin during Late Jurassic to Cretaceous time (Zhang *et al.*, 2005; Cao *et al.*, 2008), with further rifting during the Cenozoic followed by a final stage of inversion (Ritts *et al.*, 1999). Hydrocarbon source rocks occur in the Middle Jurassic succession and include the coal-bearing Dameigou and Shimengou Formations (Fig. 2) (e.g. Li *et al.*, 2016; Ritts *et al.*, 1999); Oligocene and Miocene hypersaline lacustrine rocks also have source rock potential (e.g. Hanson *et al,,* 2001) but are not considered here.

The present study focuses on Middle Jurassic lacustrine shales in a study area in the northern Qaidam Basin. Previous research on Middle Jurassic organic-matter rich deposits in this area have in general focussed on sequence stratigraphy and palaeogeography (Li *et al.*, 2014, 2016), and the assessment of coal resources (Lu *et al.*, 2009); a few studies of oil and gas resources (Bao *et al.*, 2013; Hou *et al.*, 2017a; Wang *et al.*, 2015) and the related source rocks have been made (Li *et al.*, 2008; Hou *et al.*, 2017b; Ritts *et al.*, 1999). However, previous source rock studies were in general based on limited numbers of shale samples and focussed on the Middle Jurassic Dameigou Formation (e.g. Ritts *et al.*, 1999). In contrast, few studies have investigated the palaeodepositional environment and source rock

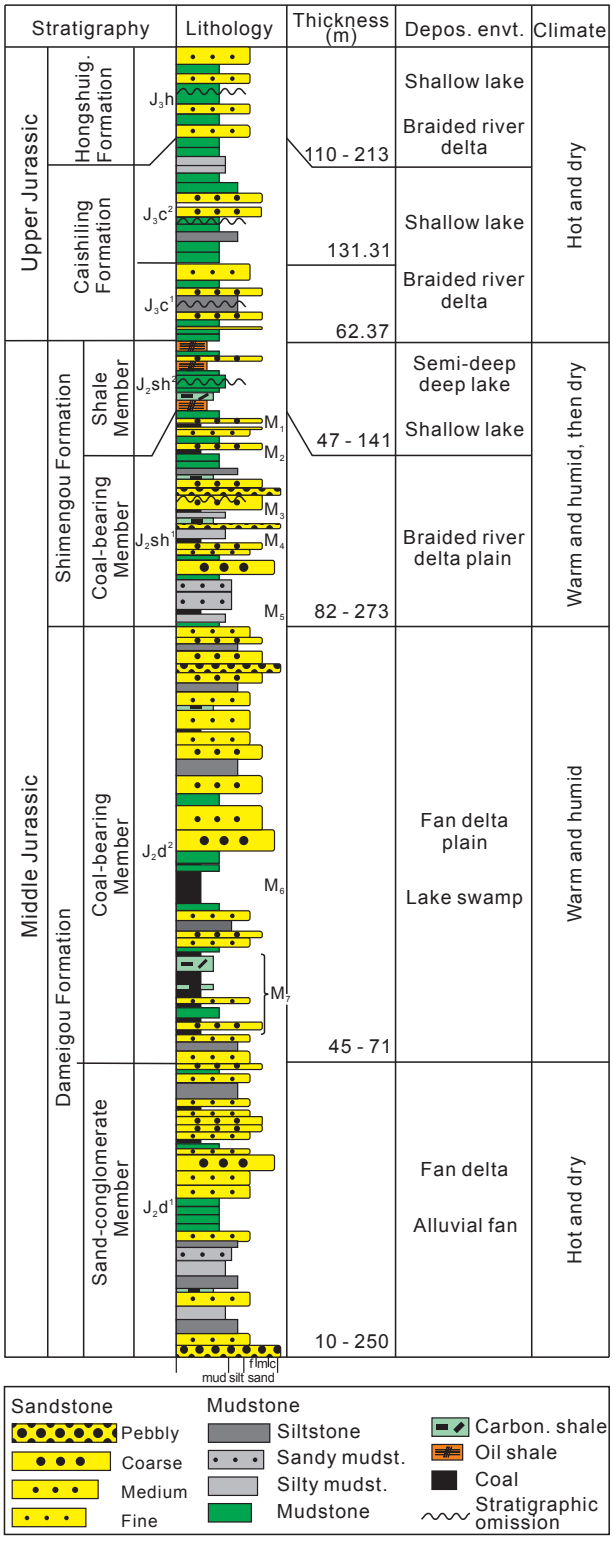

Fig. 2. Lithostratigraphy of the Middle – Upper Jurassic succession in the northern Qaidam Basin (modified after Shao *et al.*, 2014).

potential of lacustrine sediments in the upper part of the Shimengou Formation, referred to here as the Shale Member (Fig. 2).

The aim of this paper is to apply bulk geochemical parameters in combination with maceral, biomarker and compound-specific isotope data to reconstruct the depositional environment of the Shale Member of the Shimengou Formation and to quantify its petroleum potential.

Geological setting

The Qaidam Basin (Fig. 1) is bounded by the ENE-WSW striking Altyn Tagh strike-slip fault in the NW, the NW-SE striking Elashan strike-slip fault in the

east, and the Kunlun fault in the south (Fig. 1b). The northern part of the Qaidam Basin is characterized by a series of sub-basinal depressions and interior uplifts which developed at the end of the Late Triassic after the Indosinian orogeny (Chen *et al.*, 2012; Li *et al.*, 2016). Among these sub-basins is the Saishiteng Depression (Fig. 1c) in which there is a thick, non-marine Middle Jurassic coal- and shale-bearing succession. Basement is composed of Upper Ordovician magmatic and metamorphic rocks (Li *et al.*, 2016). The Middle Jurassic consists of the Dameigou Formation, up to 320 m thick, and the overlying Shimengou Formation which is divided into the lower Coal-bearing Member and the overlying Shale Member (Fig. 2). Fluvial and deltaic deposits with coal seams dominate the Dameigou Formation and the Coal-bearing Member of the Shimengou Formation, whereas fine-grained sediments are present in the Shale Member (Li *et al.*, 2016). According to Li *et al.* (2016), the Shale Member was deposited during a time of increasing basement subsidence in a lake with varying water depths, which is referred to here as the Shimengou Lake.

The Shale Member is 47 to 141 m thick (Fig. 2) and its thickness increases southwards (Li *et al.*, 2016). Based on the ratio of coarse- to fine-grained sediments and the thickness of mudstone intervals, Li *et al.* (2016) distinguished a shallow lake facies (coarse/fine ratio >0.3; mudstone thickness <25 m) along the northern basin margin, from a deep lake facies. The shallow lake facies is mainly composed of longshore bar deposits, characterized by fine-grained sandstones with low-angle cross bedding and greyish bioturbated siltstones. Mudstones from the shallow lake facies are typically black, laminated and often contain bivalves and woody fragments. The deep lake facies is composed of dark mudstones including organic-matter rich black shales and black-brown oil shales. The latter term is used in China for organic-matter rich rocks which on low-temperature distillation yield more than 3.5 % oil (Liu *et al.*, 2009).

SAMPLES AND METHODS

A total of 88 core samples (69 mudstones, eight oil shales, 10 silty mudstones and one siltstone) were recovered from borehole QD-1 (Fig. 1c) over the depth interval 14.9 to 260.0 m (measured depth; MD). Sampling positions are indicated in Fig. 3. Because Jurassic strata in the study area dip at about 70°, MD and true stratigraphic thickness (TD) differ considerably, and TD is used in the present paper. The sampled interval (5-90 m TD) corresponds to the entire Shale Member of the Shimengou Formation.

All samples were subjected to bulk geochemical analyses. Organic petrographic (24 samples), biomarker (28 samples) and compound specific carbon isotope analyses (11 samples) were applied to subsets of the samples.

Total carbon and total sulphur contents were measured on powdered sample material (<250 μm) using a LECO C/S analyzer before the total organic carbon (TOC) contents were determined on the residues using the same instrument. Total inorganic carbon (TIC) contents were derived from the differences between TC and TOC. Variations in calcite equivalent percentages within the succession were calculated ($calc_{eq}$ = 8.34 x TIC) from the data. Depending on the TOC content, 10 to 50 mg of each sample was analysed by Rock-Eval pyrolysis on a Vinci Rock-Eval 6 instrument. Based on TOC and Rock-Eval data and the position within the well, samples were selected for maceral and biomarker analyses and stable isotope analysis of TOC and carbonate.

Microscopic analysis was performed on polished blocks of whole rock cut perpendicular to bedding using a Leica MPV microscope and oil immersion objectives. Maceral analysis was performed by a single-scan method (Taylor *et al.*, 1998) using reflected white and fluorescent light and a 50× objective. At least 1000 points per polished block were counted.

For biomarker analysis, accelerated solvent extraction of crushed samples by dichloromethane was applied (Dionex ASE 200; 1 h, 75°C, 75 bar). Asphaltenes were precipitated from a hexane-DCM solution (80:1) and separated by centrifugation. Subsequently, polar compounds and saturated and aromatic hydrocarbons were separated by medium pressure liquid chromatography (MPLC) using a Köhnen-Willsch instrument (Radke *et al.*, 1980).

The hydrocarbon fractions were analyzed by gas chromatography – mass spectrometry (Trace-GC with a 60 m DB-5MS column (i.d. 0.25 mm; 0.25 μm film thickness) coupled to a ThermoFisher ISQ quadrupole mass spectrometer). The oven temperature gradient was programmed from 40 to 310°C at 4°C/min, followed by an isothermal period of 40 min. Helium was used carrier gas. The mass spectrometer was operated in the EI (electron ionization) mode over a scan range from *m/z* 50 to 600 (0.5 s total scan). Data were processed using an Xcalibur data system. Concentrations of different compound groups in the saturated and aromatic hydrocarbon fractions were calculated using peak areas from the gas chromatograms in relation to those of internal standards (deuterated *n*-tetracosane and 1,1′-binaphthyl, respectively). The concentrations were normalized to the TOC content.

Carbon isotope measurements on specific compounds in the saturated hydrocarbon fractions of selected samples were performed using a Trace-GC instrument attached to a ThermoFisher DELTA-V isotope ratio mass spectrometer via a combustion interface (GC Isolink, ThermoFisher). The GC column

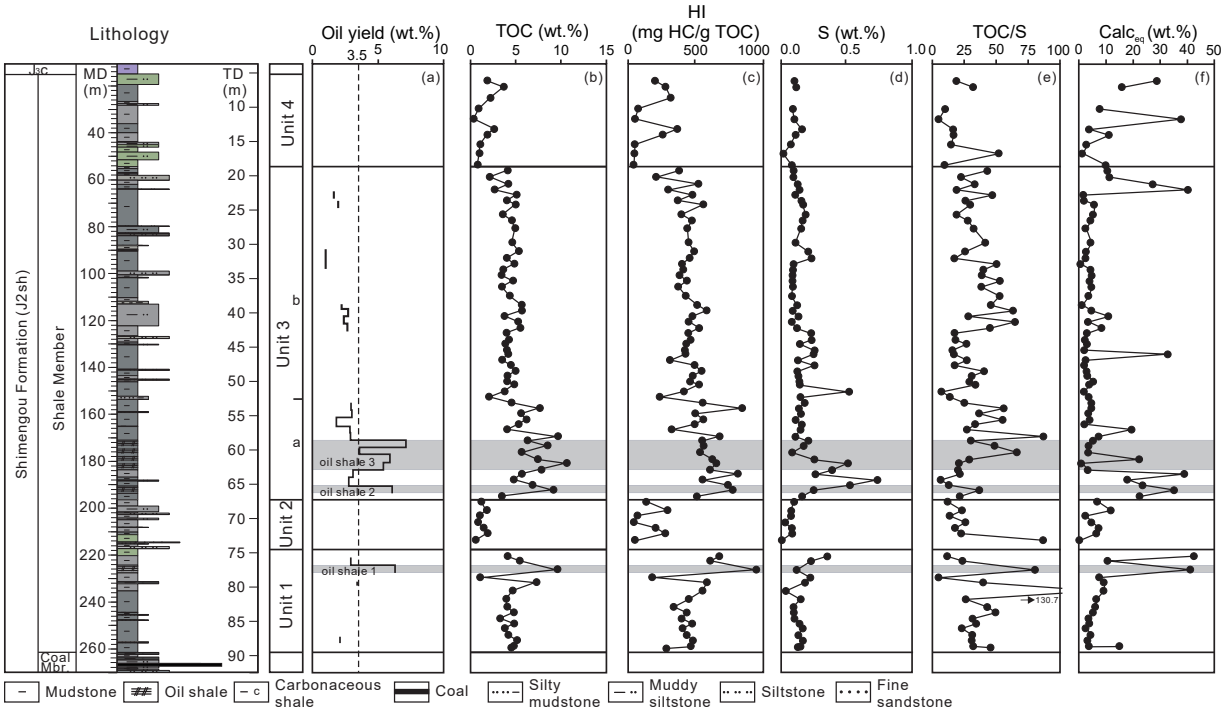

Fig. 3. Depth profiles of bulk geochemical proxies in the Shale Member of the Shimengou Formation. Oil shale layers are numbered from bottom to top. MD, measured depth; TD, true stratigraphic depth; TOC, total organic carbon; HI, hydrogen index; Calc$_{eq}$, calcite equivalent; S, sulphur; Mbr., Member.

and temperature programme were the same as that used for GC–MS analysis. Stable isotope ratios were measured against commercial CO_2 as a monitoring gas, calibrated by -NBS-19 reference material, and reported in standard delta notation ($\delta^{13}C$; Coplen, 2011) relative to Vienna-Pee Dee Belemnite, V-PDB, where $\delta^{13}C = (^{13}C/^{12}C)_{sample} / (^{13}C/^{12}C)_{standard} - 1$). The analytical error was better than 0.2‰.

Oil yield gained from low temperature carbonization (~520°C) of 1 m long core intervals was measured by a Fushun retort using the Fischer assay method (Liu *et al.*, 2009). A mixture of oil and water was extracted from oil shale by heating, and then add xylene into the mixture, heat it until it is boiled, and the oil and water were seperated according to different boiling point, the content of oil was obtained by weighing the water distilled from the mixture. According to Chinese terminology (Liu *et al.*, 2009), an oil shale is defined by an oil yield exceeding 3.5 wt % on low-temperature distillation.

RESULTS AND INTERPRETATION

Bulk geochemical parameters and organic petrology

Bulk geochemical data and maceral percentages of samples from the Shale Member of the Shimengou Formation are listed in Appendix 1 (p. 57). Based on variations of TOC contents with depth, four sedimentary units were differentiated in the Shale Member are referred as Units 1 to 4 from base to top (Fig. 3). These units are discussed separately in the following section. T_{max} values in the units vary between 423 and 439 °C (Fig. 4) and do not show a clear trend versus depth. Representative photomicrographs of organic particles are shown in Fig. 5. Vertical variations versus depth of the sum of terrigenous macerals (vitrinite, inertinite, sporinite), of telalginite and of lamalginite on a mineral matter free (mmf) basis in Units 1 to 4 are plotted in Fig. 6a.

Unit 1 (89.6 – 74.3 m)

Unit 1 is mainly composed of black and dark grey mudstones, intercalated with several thin layers of muddy siltstones. Samples from Unit 1 have an average TOC of 4.7 wt.% (Fig. 3), and the highest TOC content (9.6 wt.%; Fig. 3b) is observed in an interval which has an oil yield >3.5 wt.%, and which is referred to here as "oil shale Layer 1" (TD: 2.06 m). HI values range from 179 to 676 mg HC/g TOC, but reach 952 mg HC/g TOC in this interval (Fig. 3c). Consequently, the organic matter in Layer 1 is classified as Type I kerogen, whereas most of the mudstones in the unit contain Type II kerogen (Fig. 4). This kerogen classification is supported by high quantities of aquatic macerals (lamalginite and telalginite); lamalginite (44-48 vol.%) dominates over telalginite. The relative percentage of the latter maceral increases upwards at the expense of terrigenous macerals, which occur in only minor quantities.

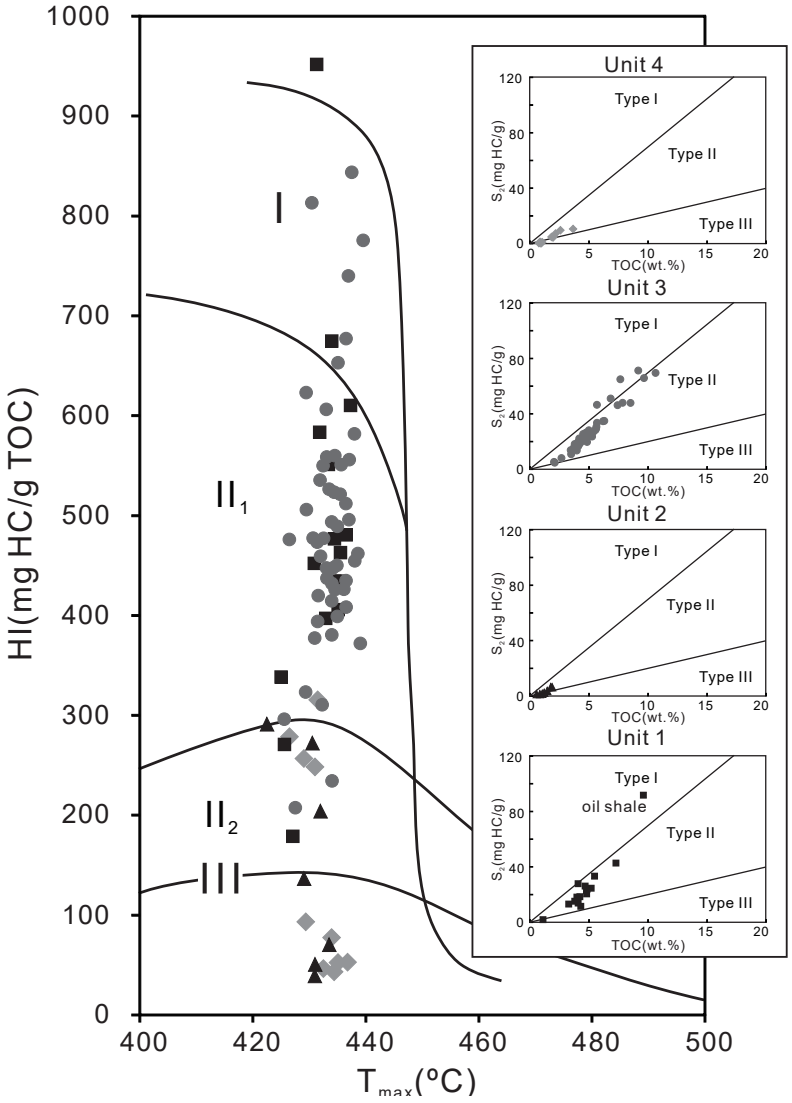

Fig. 4. Plots of HI versus T_{max} (according to Espitalié *et al.*, 1984) outlining kerogen types in the Shale Member of the Shimengou Formation. S_2 versus TOC correlations for Units 1– 4 are shown as inserts (according to Langford and Blanc-Valleron, 1990).

Sulphur contents are low in Unit 1 samples (< 0.4 wt.%; Fig. 3d) resulting in high TOC/S ratios (23.0–130.7) except for one OM-lean mudstone sample from 78.5 m depth (Fig. 3e). Carbonate contents are generally low (< 10 wt.%$calc_{eq}$), but are elevated in oil shale and mudstone samples near the base and the top of Unit 1 (Fig. 3f).

Unit 2 (74.3 – 67.1 m)

Unit 2 is composed of grey and greyish-green mudstones, intercalated with thin layers of siltstones, muddy siltstones and silty mudstones. TOC (0.6–1.9 wt.%; Fig. 3b) and HI values (52–294 mg HC/g TOC; Fig. 3c) are relatively low in samples from Unit 2. A classification of the organic material as Type III kerogen is supported by the HI values (Fig. 4) and the dominance of land-plant derived macerals (94–8 vol. %). Inertinite and vitrinite, both with small particle size, were the most frequent macerals recorded.

The low sulphur contents (<0.2 wt.%; Fig. 3d) result in high TOC/S ratios (up to 86.9; Fig. 3e) and show a subtle upwards increase. Carbonate contents (0.2–22.4 wt.%$calc_{eq.}$) increase in the same direction (Fig.3f).

Unit 3 (67.1 – 18.6 m)

Unit 3 is characterized by two oil shale layers and dark grey mudstones, intercalated with siltstones, muddy siltstones and silty mudstones. TOC contents and HI values in samples from Unit 3 range from 2.0 to 10.7 wt.% (average: 5.1 wt.%), and from 208 to 845 mg HC/g TOC, respectively (Figs 3b, c). Both the highest TOC (3.5–10.7 wt.%) and the highest HI values (324–845 mg HC/g TOC; Type II and I kerogen) occur in the lower part of the unit (67.1–52.6 m) in Unit 3a (Fig. 3). Oil yield data (Fig. 3a) indicate that two intervals in the lower part of Unit 3a have an oil yield >3.5 wt.%; these intervals are referred to as oil shale "Layers 2

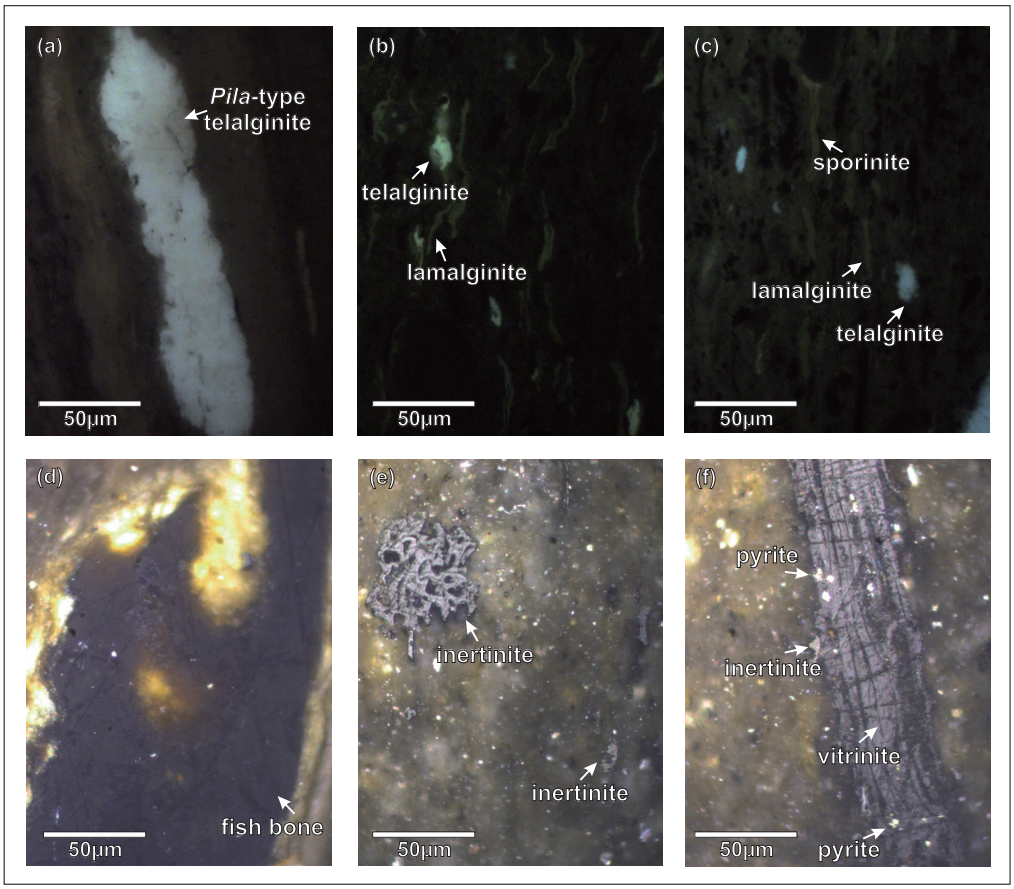

Fig. 5. Photomicrographs of samples from the Shale Member of the Shimengou Formation: (a) sample Ty-63, UV light; (b) sample Ty-79, UV light; (c) sample Ty-74, UV light; (d) sample Ty-63, white light; (e) sample Ty-75, white light; (f) Ty-75, white light.

and 3" (TD: 2.03 m and 8.03 m, respectively). Maceral compositions in Unit 3a are characterized by very high percentages of alginite (>70 vol.%). Telalginite (including Pila-type algae; Fig. 5a) is more abundant than lamalginite in the lower part of the unit, but the percentage of telalginite decreases upwards. Fish bones are abundant in oil shale samples (Fig. 5d).

The interval between 52.6 and 18.6 m depth (Unit 3b) is characterized by TOC contents of about 4.5 wt.% and HI values around 400 mg HC/g TOC, showing the presence of Type II kerogen (Fig. 4). Although terrigenous macerals (mainly inertinite and vitrinite (Figs. 5e,f) with subordinate sporinite; <2 vol.%) occur in higher amounts (23–46 vol.%) than in Unit 3a, alginite (mainly lamalginite) remains the most frequent maceral type. Vitrinite often contains framboidal pyrite (Fig. 5f).

Sulphur contents are generally low with maximum values (~0.7 wt%) in Unit 3a (Fig. 3d). TOC/S ratios are high throughout Unit 3 (7–87), but an abrupt upward increase in TOC/S ratios occurs at 42.6 m depth (Fig. 3e). TOC/S ratios decrease upwards above this depth.

Carbonate contents in Unit 3 are often low, but samples with up to 38.9 wt.% $calc_{eq}$ occur in Unit 3a and in the uppermost part of Unit 3b (Fig. 3f)

Unit 4 (18.6–5.1 m)

Unit 4 is dominated by grey, greyish-green mudstones intercalated with muddy siltstones, which are characterized by relatively low organic matter contents (average: 1.7 wt.%) (Fig. 3b). Rock-Eval HI values ranging from 43 to 317 mg HC/g TOC (Fig. 3b) and abundant land plant-derived macerals (57–98 vol.%) confirm the presence of Types III and II kerogen (Fig. 4). Sulphur contents are very low (<0.2 wt.%; Fig. 3d) and TOC/S ratios are high (9.6–52.1; Fig. 3e). The carbonate contents vary between 1.3 and 37.9 wt.% $calc_{eq}$ (Fig. 3f).

Organic geochemistry

The amount of extractable organic matter (EOM) in the samples analysed varies between 10 and 49 mg/g TOC (Table 1). The proportion of hydrocarbons ranges between 33 and 62% of the EOM. Saturated hydrocarbons (23–41% of the EOM) in general dominate over aromatic hydrocarbons (4–33 % of EOM). In addition, the EOM includes NSO compounds (35–64 % of EOM) and asphaltenes (1–12 % of EOM; Table 1). Total ion chromatograms (TICs) of saturated and aromatic hydrocarbon fractions of representative samples from the Shale Member of the Shimengou Formation are shown in Fig. 7. The concentrations

Table 1. Bulk organic geochemical data.

Samples	MD (m)	TD (m)	Lithology	EOM[a] (mg/g TOC)	Saturated HC[b] (wt%, EOM)	Aromatic HC[b] (wt%, EOM)	NSO[c] (wt%, EOM)	Asphaltenes (wt%, EOM)
Ty-136	25.1	8.6	mudstone	40	41	10	41	8
Ty-132	38.4	13.1	mudstone	30	28	15	49	8
Ty-129	48.7	16.6	mudstone	49	29	33	36	3
Ty-125	61.7	21.1	mudstone	13	25	11	52	12
Ty-118	80.7	27.6	mudstone	10	35	18	39	8
Ty-116	90.4	30.9	mudstone	13	23	11	55	11
Ty-110	105.5	36.1	mudstone	16	35	14	47	5
Ty-104	123.1	42.1	mudstone	13	32	13	48	7
Ty-98	136.7	46.8	mudstone	16	33	13	42	12
Ty-96	141.5	48.4	mudstone	13	26	8	56	10
Ty-92	150.2	51.4	mudstone	15	33	15	47	5
Ty-90	155.0	53.0	mudstone	13	28	6	60	6
Ty-86	164.1	56.1	mudstone	10	38	15	42	5
Ty-83	171.1	58.5	oil shale	22	31	15	48	5
Ty-81	176.0	60.2	oil shale	12	29	26	40	6
Ty-79	180.7	61.8	oil shale	10	34	10	50	6
Ty-77	185.3	63.4	mudstone	31	27	12	58	3
Ty-76	187.8	64.2	mudstone	10	28	14	52	6
Ty-74	192.1	65.7	oil shale	27	35	9	53	4
Ty-73	194.8	66.6	mudstone	36	35	8	53	4
Ty-72	197.1	67.4	mudstone	23	33	14	44	9
Ty-69	205.9	70.4	mudstone	23	39	17	35	9
Ty-66	213.5	73.0	mudstone	28	40	19	40	1
Ty-63	226.1	77.3	oil shale	46	26	9	64	2
Ty-62	229.4	78.4	mudstone	30	35	15	44	6
Ty-61	231.5	79.2	mudstone	19	29	10	55	6
Ty-58	241.9	82.7	mudstone	11	29	4	61	6
Ty-55	249.1	85.2	mudstone	16	36	12	47	5

MD: measured depth; TD: true stratigraphic depth; EOM: extractable organic matter; HC: hydrocarbons; NSO: heterocompounds

and concentration ratios of compounds and compound groups in hydrocarbon fractions are listed in Table 2.

Straight chain alkanes, isoprenoids

Most samples are dominated by *n*-alkanes of intermediate (*n*-C_{21-25}) to short (*n*-C_{15-19}) chain length with a marked odd-over-even predominance, but several samples from oil shale Unit 3a (66.3–58.5 m) are characterized by high intensities of C_{21-25} and C_{27-31} *n*-alkanes, respectively (Fig. 6b). The carbon preference index (CPI; Bray and Evans, 1961) varies between 1.3 and 3.5 (Table 1). Alkanes of low molecular weight (*n*-C_{15} to *n*-C_{20}) are considered as markers for phytoplankton (algae) and microorganisms (Cranwell, 1977), whereas long-chain alkanes are the main components of plant waxes (Eglinton and Hamilton, 1967). Aquatic macrophytes are reported to be characterized by high abundances of C_{23} and C_{25} *n*-alkanes (Ficken *et al.*, 2000).

The acyclic isoprenoids pristane (Pr) and phytane (Ph) are present in all samples. Pr/Ph ratios are low and range between 0.2 and 1.1 (Fig. 6c). As the influence of varying rank on Pr/Ph ratios (Tissot and Welte, 1984) can be ruled out in the present study, the low Pr/Ph values are interpreted to indicate anaerobic conditions during deposition (Didyk *et al.*, 1978). Based on independent molecular parameters (e.g. the presence of β-carotane and aryl isoprenoids; *see below*), the low Pr/Ph values are consistent with anoxic bottom-water conditions during oil shale deposition. Enhanced Pr/Ph ratios in samples containing coaly material imply slightly higher oxygen availability and an increasing contribution by land plants on Pr/Ph values.

Steroids

Steroids are present in high concentrations in the oil shales (61.6 –964.9 μg/g TOC) and in lower contents in the mudstone samples (14.3 – 183.1 μg/g TOC) (Fig. 6d). In the saturated hydrocarbon fraction, the 5α, 14α, 17α (H) steranes are dominating over the 5β, 14α, 17α (H) isomers, and are present in the C_{27}–C_{29} range (Fig. 7). The carbon number distribution of regular steranes

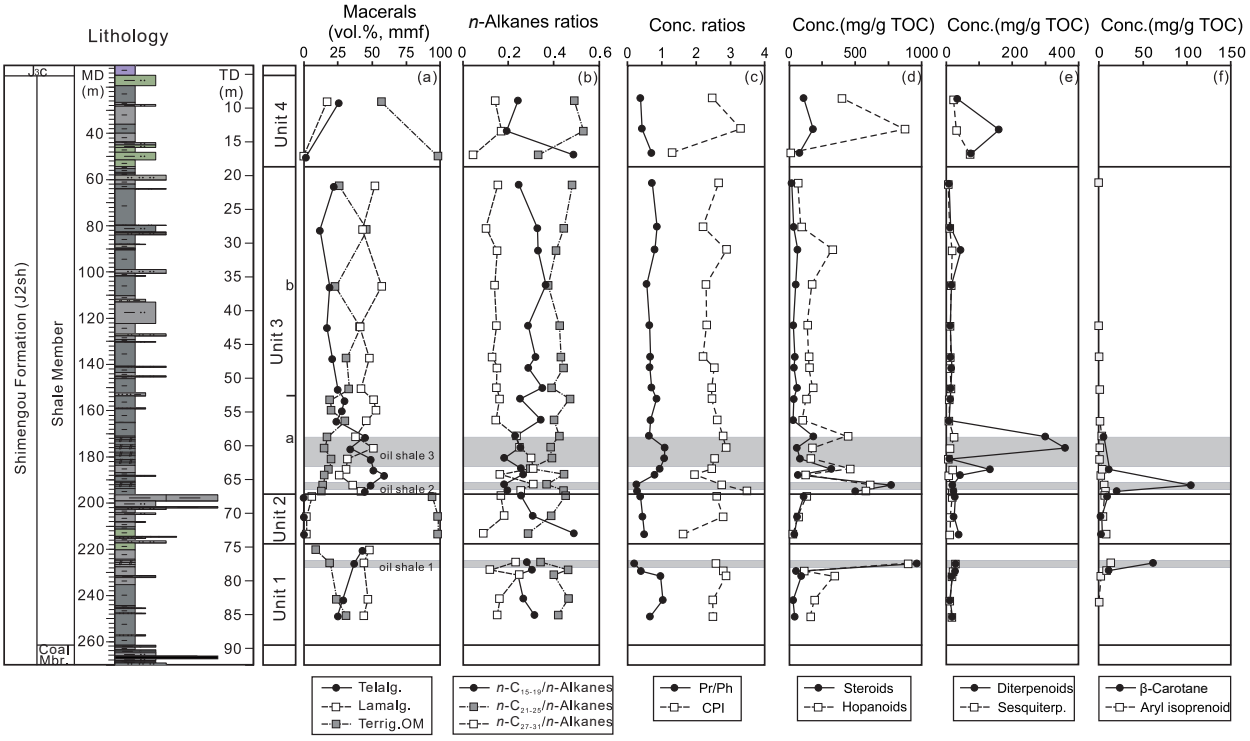

Fig. 6. Distribution versus depth of (a) macerals (telalginite, lamalginite, terrigenous OM), (b) ratios of short (*n*-C_{15-19}), intermediate (*n*-C_{21-25}) and long-chain (*n*-C_{27-31}) *n*-alkanes to the sum of *n*-alkanes, (c) pristane/phytane ratios and carbon preference index, (d) steroid and hopanoid concentrations, (e) diterpenoid and sesquiterpenoids, (f) β-carotane and aryl isoprenoid concentrations within the Shale Member of the Shimengou Formation. MD, measured depth; TD, true stratigraphic depth.

is C_{27}>C_{29}>C_{28} for the samples from organic-lean units (Units 2 and 4), whereas in the organic-rich units (Units 1 and 3), C_{29} steranes predominate in several samples. The aromatic fraction is dominated by a considerable concentration of monoaromatic steroids in all samples (5.5 – 48.9 μg/g TOC; Fig. 8).

C_{27} sterols are found mostly in algal organic matter and zooplankton, while land plants or freshwater microalgae dominantly contain C_{29} sterols (Volkman, 1986; Kodner *et al.*, 2008). The C_{28} sterols are thought to be derived from various sources (Grantham and Wakefield, 1988; Peters *et al.*, 1989, 2000). In the present case, the change in carbon number distribution of steranes from C_{27}- to C_{29}-dominance in Units 2 and 4 occurs in the same depth interval as the change in the predominance of short to intermediate molecular weight *n*-alkanes (Table 2), which may indicate an increased contribution from microalgae (Volkman *et al.*, 1998) and macrophytes. A ternary diagram outlining the relative proportions of C_{27}, C_{28} and C_{29} steranes (Fig. 9) indicates a mixed algal-terrigenous source of OM.

Hopanoids

The hopanoid patterns are characterized by 17α, 21β and 17β, 21βhopanes from C_{27} to C_{31}, with C_{28} hopanes absent. C_{27} and C_{29} hop-17(21)-enes are also present. Predominant triterpenoids are the 17α, 21β-C_{29}hopane, 17α, 21β-C_{30}hopane, and 17β, 21β-C_{31}hopane (Fig. 7). Hopanoids are present in high concentrations in oil shales (164.9–896 μg/g TOC) and in generally lower abundances in the mudstones (16.2–876.3 μg/g TOC) (Fig. 6d). Bacteriohopanepolyols found in bacterial biomass are considered to be the main biological precursors of hopanoids (Ourrison *et al.*, 1979; Rohmer *et al.*, 1992). The 22S/(22S+22R) isomer ratios of the 17α, 21β-C_{31}hopanes vary between 0.1 and 0.3. Benzohopanes occur in all samples in relatively low amounts (1.4–34.7 μg/g TOC) (Fig. 8). These compounds are also attributed to bacterial activity (Hussler *et al.*, 1984).

Land plant related hydrocarbons

Diterpenoids (including α-phyllocladane, abietatetraene, simonellite and retene) occur in variable concentrations in the oil shale Unit 3a (10.3–448.4 μg/g TOC) and in Unit 4 (42.5–198.7 μg/g TOC), but in general show lower abundances in Units 1, 2 and 3b (10.4-55.0 μg/g TOC) (Table 2; Fig. 6e). Sesquiterpenoids (e.g. cuparene, curcumene, tetrahydrocadalene, cadalene and isocadalene) occur in lower amounts (9.2–90.8 μg/g TOC) (Table 1; Fig. 6e) and are only enriched in Unit 4. Diterpenoids and sequiterpenoids indicate a contribution by conifer species (Otto *et al.*, 1997; Otto and Wilde, 2001). The predominance of gymnosperms (mainly conifers)

Table 2. Biomarker concentrations and concentration ratios.

Samples	MD (m)	TD (m)	*n*-C_{15-19} /*n*-alk. (-)	*n*-C_{21-25} /*n*-alk. (-)	*n*-C_{27-31} /*n*-alk. (-)	CPI (-)	Pr/*n*-C_{17} (-)	Ph/*n*-C_{18} (-)	Pr/Ph (-)	Steroids (µg/g TOC)	C_{27} steranes/steranes (-)	C_{28} steranes/steranes (-)	C_{29} steranes/steranes (-)	Hopanes (µg/g TOC)	Benzohopanes (µg/g TOC)	Sesquiterp. (µg/g TOC)	Diterpenoids (µg/g TOC)	β-Carotane (mg/g TOC)	Aryl isoprenoids (µg/g TOC)
Ty-136	25.1	8.6	0.24	0.49	0.14	2.48	0.64	1.37	0.38	112.0	0.45	0.25	0.30	337.75	8.3	28.0	42.5		
Ty-132	38.4	13.1	0.19	0.53	0.17	3.30	0.89	1.68	0.43	183.1	0.49	0.18	0.33	746.29	23.5	40.7	198.7		
Ty-129	48.7	16.6	0.49	0.33	0.05	1.30	0.56	0.68	0.70	81.3	0.54	0.21	0.25	10.11	2.7	90.8	93.9		
Ty-125	61.7	21.1	0.25	0.48	0.15	2.67	0.72	0.85	0.72	23.0	0.33	0.20	0.47	53.85	9.5	9.2	10.4		0.4
Ty-118	80.7	27.6	0.33	0.44	0.10	2.20	0.82	0.87	0.86	36.6	0.39	0.18	0.43	71.70	12.1	14.1	16.1		
Ty-116	90.4	30.9	0.33	0.41	0.15	2.89	0.90	1.09	0.80	66.3	0.36	0.18	0.46	261.55	23.5	22.9	55.0		
Ty-110	105.5	36.1	0.37	0.37	0.14	2.29	0.96	1.50	0.57	52.6	0.53	0.16	0.32	131.96	19.9	19.9	18.8		
Ty-104	123.1	42.1	0.29	0.43	0.15	2.31	0.75	1.09	0.64	34.4	0.33	0.21	0.45	107.75	18.6	16.6	15.0		0.3
Ty-98	136.7	46.8	0.32	0.43	0.13	2.20	0.83	1.06	0.67	45.5	0.37	0.17	0.46	115.97	17.3	17.2	18.0		0.3
Ty-96	141.5	48.4	0.29	0.44	0.15	2.53	0.86	1.09	0.65	38.6	0.35	0.18	0.47	118.46	18.0	15.9	20.2		
Ty-92	150.2	51.4	0.35	0.39	0.15	2.45	1.00	1.21	0.71	62.1	0.49	0.13	0.38	135.86	21.7	19.1	17.5		0.5
Ty-90	155.0	53.0	0.25	0.47	0.16	2.46	0.22	0.22	0.85	38.0	0.32	0.22	0.46	97.26	19.2	12.7	14.7		
Ty-86	164.1	56.1	0.34	0.40	0.15	2.62	1.00	1.28	0.67	33.0	0.43	0.20	0.38	79.67	11.3	11.6	10.3		0.9
Ty-83	171.1	58.5	0.23	0.42	0.24	2.79	0.79	1.91	0.64	185.3	0.40	0.20	0.40	351.72	22.8	31.0	373.8	4.7	3.4
Ty-81	176.0	60.2	0.25	0.39	0.25	2.87	0.96	0.98	1.08	61.6	0.36	0.21	0.43	130.77	23.5	14.3	448.4		0.9
Ty-79	180.7	61.8	0.18	0.39	0.30	2.54	0.95	0.86	1.08	84.4	0.32	0.20	0.48	126.63	12.2	8.0	12.1		0.7
Ty-77	185.3	63.4	0.26	0.30	0.31	2.46	1.84	1.93	0.94	320.5	0.42	0.19	0.39	306.39	34.7	24.2	165.7	11.0	3.9
Ty-76	187.8	64.2	0.27	0.44	0.16	1.96	1.47	1.71	0.80	68.5	0.33	0.20	0.47	96.09	10.0	10.9	53.3		1.8
Ty-74	192.1	65.7	0.18	0.37	0.31	2.75	1.34	4.95	0.27	771.4	0.65	0.11	0.25	333.02	8.2	17.8	24.1	104.3	5.4
Ty-73	194.8	66.6	0.20	0.44	0.25	3.49	0.93	3.13	0.28	500.2	0.61	0.13	0.26	368.53	7.9	21.8	28.0	20.1	7.1
Ty-72	197.1	67.4	0.26	0.45	0.17	2.60	1.17	2.71	0.38	112.0	0.65	0.11	0.24	85.14	8.9	23.3	33.7	9.1	5.9
Ty-69	205.9	70.4	0.31	0.39	0.18	2.79	1.06	1.79	0.44	62.8	0.59	0.14	0.27	48.20	4.2	16.6	29.0	2.2	4.3
Ty-66	213.5	73.0	0.49	0.29	0.09	1.63	0.83	1.26	0.50	42.4	0.61	0.15	0.24	20.84	1.4	14.2	47.7	2.5	7.9
Ty-63	226.1	77.3	0.28	0.34	0.23	2.58	1.22	5.93	0.20	964.9	0.64	0.14	0.23	518.21	8.2	35.0	36.1	61.2	13.2
Ty-62	229.4	78.4	0.30	0.46	0.12	2.79	1.23	2.62	0.39	56.3	0.56	0.17	0.27	89.11	5.3	27.0	35.3	11.1	8.5
Ty-61	231.5	79.2	0.24	0.40	0.25	2.87	0.97	1.18	0.97	94.2	0.42	0.19	0.39	271.03	28.7	23.2	21.4		2.3
Ty-58	241.9	82.7	0.27	0.46	0.16	2.49	0.60	0.59	1.03	31.5	0.35	0.19	0.46	156.50	17.0	16.1	14.2		0.3
Ty-55	249.1	85.2	0.32	0.42	0.15	2.49	0.85	1.10	0.66	44.2	0.43	0.15	0.42	122.66	19.2	22.3	23.0		

MD: measured depth; TD: true stratigraphic depth; CPI: carbon preference; Pr/Ph: pristane/phytane ratio; Sesquiterp.: sesquiterpenoids.

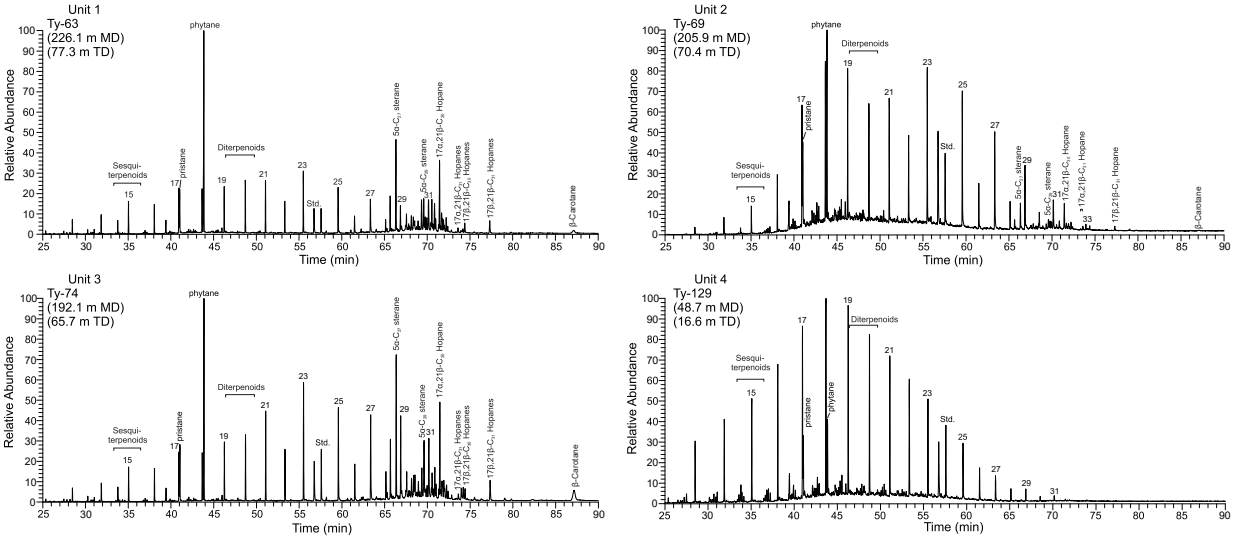

Fig. 7 Gas chromatograms (TICs) of saturated hydrocarbon fractions of samples from the four units of the Shale Member of the Shimengou Formation. *n*-Alkanes are labelled according to their carbon number. Std., standard (deuteriated *n*-tetracosane).

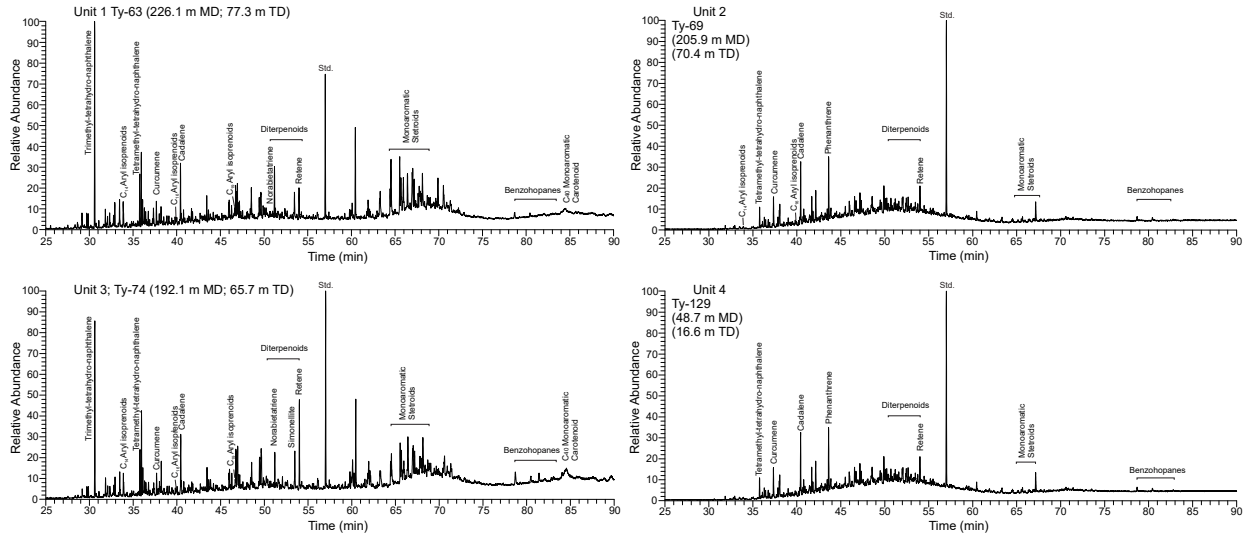

Fig. 8. Gas chromatograms (TICs) of aromatic hydrocarbon fractions of samples from the four units of the Shale Member of the Shimengou Formation. Std., standard (1,1'-binaphthyl).

in the palaeovegetation is also supported by pollen assemblages (Wang *et al.*, 2005).

Carotenoids

β-carotane is present in considerable quantities (4.7–104.3 μg/g TOC; Table 2) in sediments from the top of Unit 1 to the bottom of Unit 3 (Fig. 6f). Because carotenoids are easily oxidized, they are rarely found in sediments (Repeta and Gagosian, 1987; Repeta, 1989). However, under highly reducing conditions, the carotenoid skeleton may be preserved in sedimentary rocks (Peters *et al.*, 2005). The aromatic hydrocarbon composition is further characterized by the occurrence of C_{14}, C_{16} and C_{19} aryl isoprenoids (Fig. 8) in most samples, with the C_{14} aryl isoprenoids in the highest abundance (Fig. 8). These compounds are present in elevated concentrations (3.4–13.2 μg/g TOC) in the same stratigraphic units which contain β-carotane (Fig. 6f), but also occur in Unit 3b in very low amounts. Beside their origin from carotenoids specific for photosynthetic green sulphur bacteria (Chlorobiaceae; Summons and Powell, 1987), aryl isoprenoids have been reported as diagentic products from β-carotane by Koopmans *et al.*, (1996). However, the occurrence of β-isorenieratane in the oil shale sample at 77.3 m depth, suggests that the aryl isoprenoids are most probably derived from green sulphur bacteria (Brocks and Schaeffer, 2008; Bechtel *et al.*, 2018).The occurrence

Table 3. Data from compound specific stable isotope geochemistry.

Sample	MD	TD	*n*-C_{15}	*n*-C_{16}	*n*-C_{17}	Pristane	*n*-C_{18}	Phytane	*n*-C_{19}	*n*-C_{20}	*n*-C_{21}	*n*-C_{22}	*n*-C_{23}	*n*-C_{24}	*n*-C_{25}	*n*-C_{26}	*n*-C_{27}	*n*-C_{28}	*n*-C_{29}	C_{27}-Sterane	C_{29}-Sterane	aβ C_{30}-Hopane	aβC_{31}-Hopane (R)	ββ C_{30}-Hopane	ββ C_{31}-Hopane	Hop-17(21)-ene
	(m)	(m)	(δ13C, ‰, PDB)																							
Ty-129	48.7	16.6	-28.3	-28.2	-28.3	-28.7	-28.7	-29.4	-29.2	-29.6	-29.9	-30.2	-30.0	-29.1	-29.5	-30.2	-30.3	-29.8	-29.9							
Ty-125	61.7	21.1	-30.4	-30.6	-30.6	-30.1	-31.3	-29.8	-31.9	-32.3	-32.8	-32.7	-33.1	-33.1	-33.4	-32.8	-33.3	-33.1	-33.4	-30.6	-29.9					
Ty-110	105.5	36.1	-30.2	-29.9	-30.3	-30.7	-30.5	-30.6	-31.1	-30.4	-30.8	-31.6	-32.2	-33.0	-33.1	-32.8	-33.0	-33.0	-33.5	-30.0	-30.5	-36.1	-35.7	-31.9	-31.5	-42.9
Ty-98	136.7	46.8	-31.0	-30.7	-30.9	-30.4	-31.6	-30.7	-32.2	-32.0	-32.4	-32.3	-32.8	-32.7	-32.6	-32.2	-32.1	-31.8	-32.0	-30.2	-29.8	-35.5	-35.7	-32.4	-32.9	
Ty-92	150.2	51.4	-30.6	-30.7	-30.8	-30.2	-31.0	-30.7	-30.9	-31.7	-31.9	-32.4	-33.7	-33.6	-33.0	-31.9	-32.6	-31.5	-32.2	-31.0	-30.7	-34.5	-35.1	-32.3	-32.2	-40.2
Ty-83	171.1	58.5	-30.2	-30.6	-30.7	-30.9	-31.2	-31.5	-31.5	-32.4	-32.0	-32.5	-32.8	-32.9	-33.1	-32.8	-32.6	-32.1	-33.2	-31.3	-30.8	-36.3	-36.3	-33.9	-34.7	-43.5
Ty-81	176.0	60.2	-31.3	-31.4	-31.8	-31.5	-31.7	-32.5	-31.7	-32.5	-32.9	-32.5	-33.3	-32.7	-33.6	-32.5	-33.2	-32.4	-33.2	-31.1	-30.8	-36.0	-36.2	-32.3	-32.7	-40.5
Ty-79	180.7	61.8	-31.5	-31.5	-31.7	-31.4	-31.9	-32.4	-32.2	-33.0	-33.2	-32.8	-33.5	-32.6	-34.2	-33.9	-34.2	-33.1	-33.7	-31.6	-32.0	-37.3	-36.8	-34.1	-33.6	-42.6
Ty-74	192.1	65.7	-32.8	-32.9	-32.9	-32.5	-33.7	-33.1	-33.5	-34.4	-34.7	-33.3	-34.5	-33.8	-34.3	-33.8	-34.0	-34.3	-33.5	-32.2	-32.7	-38.6	-37.5	-34.8	-34.3	-47.3
Ty-63	226.1	77.3	-32.7	-32.7	-33.2	-33.1	-33.6	-33.9	-34.2	-34.1	-34.6	-34.4	-35.0	-34.4	-35.1	-34.3	-34.5	-34.8	-34.4	-32.8	-33.5	-37.5	-38.3	-35.1	-35.1	-48.1
Ty-55	249.1	85.2	-32.0	-32.2	-31.7	-31.3	-31.9	-31.8	-32.1	-32.4	-33.2	-33.8	-34.4	-33.7	-34.2	-33.5	-33.9	-32.5	-33.2	-31.8	-32.2	-36.1	-35.8	-32.8	-33.4	

MD: measured depth; TD: true stratigraphic depth;

of aryl isoprenoids within the oil shale-bearing unit is interpreted to indicate euxinic conditions in the bottom waters during deposition, as further supported by the relative low TOC/S (Fig. 3e) and the low Pr/Ph for most samples (Fig. 6c).

(iii) Compound-specific stable isotope geochemistry

The carbon isotopic compositions of *n*-alkanes, pristane and phytane, together with selected steranes and hopanoids of eleven samples from the Shale Member of the Shimengou Formation, is listed in Table 3 and plotted in Fig. 10a.

The $\delta^{13}C$ values of the *n*-C_{15} to C_{29} alkanes of the samples in general show a decrease with increasing chain length (Fig. 10a). Similar distributions have been found in leaf lipids from land plants and in terrigenous organic matter (Collister *et al.*, 1994; Köster *et al.*, 1998). In the intermediate to high molecular weight range (>*n*-C_{21}), the odd-number *n*-alkanes are slightly more depleted in ^{13}C compared to intervening even-number *n*-alkanes (Fig. 10a). Isotope values in the *n*-alkanes from the Upper Cretaceous oil shale sequence of Songliao Basin, NE China studied by Bechtel *et al.* (2012) are similar to those of the samples studied here. According to these authors, the $\delta^{13}C$ systematics obtained for the long chain *n*-alkanes indicate contributions by algae and microbial OM to even-numbered *n*-alkanes (Schouten *et al.*, 1998). The results confirm the proposed mixture of *n*-alkanes from algae/aquatic and terrigenous source material.

The $\delta^{13}C$ values of pristane and phytane vary over comparable ranges to those of the short chain *n*-alkanes (Fig. 10a). The nearly equal values of both compounds argue for a similar origin (i.e. from chlorophyll), and against a major contribution of Pr from tocopherols (Goossens *et al.*, 1984).

Reliable carbon isotope values could only be obtained for the 5α-C_{27} and 5α-C_{29}steranes. The values vary from -29.8 ‰ to -33.5 ‰ (Fig. 10a; Table 3), and both are in a range similar to that obtained for short-chain *n*-alkanes and acyclic isorpenoids. The overlapping $\delta^{13}C$ values of C_{27} and C_{29}steranes (Fig. 10a) indicate that the organic matter is derived from aquatic microorganisms and land plants (Bechtel *et al.*, 2012).

The carbon isotope composition of the C_{30} and C_{31} ββ-hopanes varies between -31.5 ‰ and -35.1 ‰ (Fig. 10a). The values are in the same range, or slightly lower than, those found for biomarkers originating from organisms in the photic zone (e.g. short chain n-alkanes, Ph, steranes), possibly suggesting a mainly cyanobacterial origin for the extended hopanoids. However, a minor contribution from other prokaryotes (e.g. chemoautotrophic or methanotrophic bacteria) is possible (Köster *et al.*, 1998).

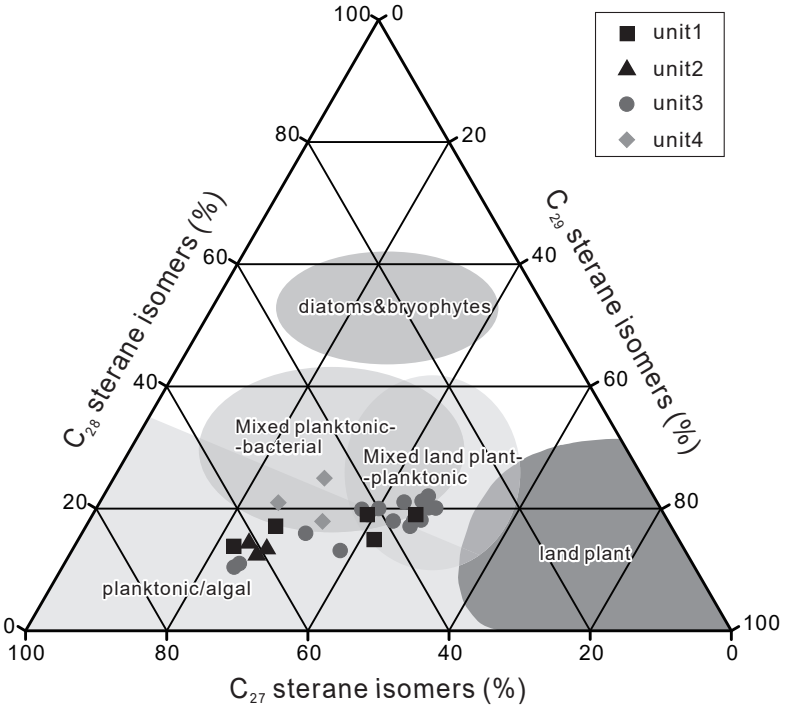

Fig. 9. Ternary plot of relative amounts of C_{27}, C_{28} and C_{29} steranes (after Hunt, 1996), indicating the different origins of the organic matter in the four units of the Shale Member of the Shimengou Formation.

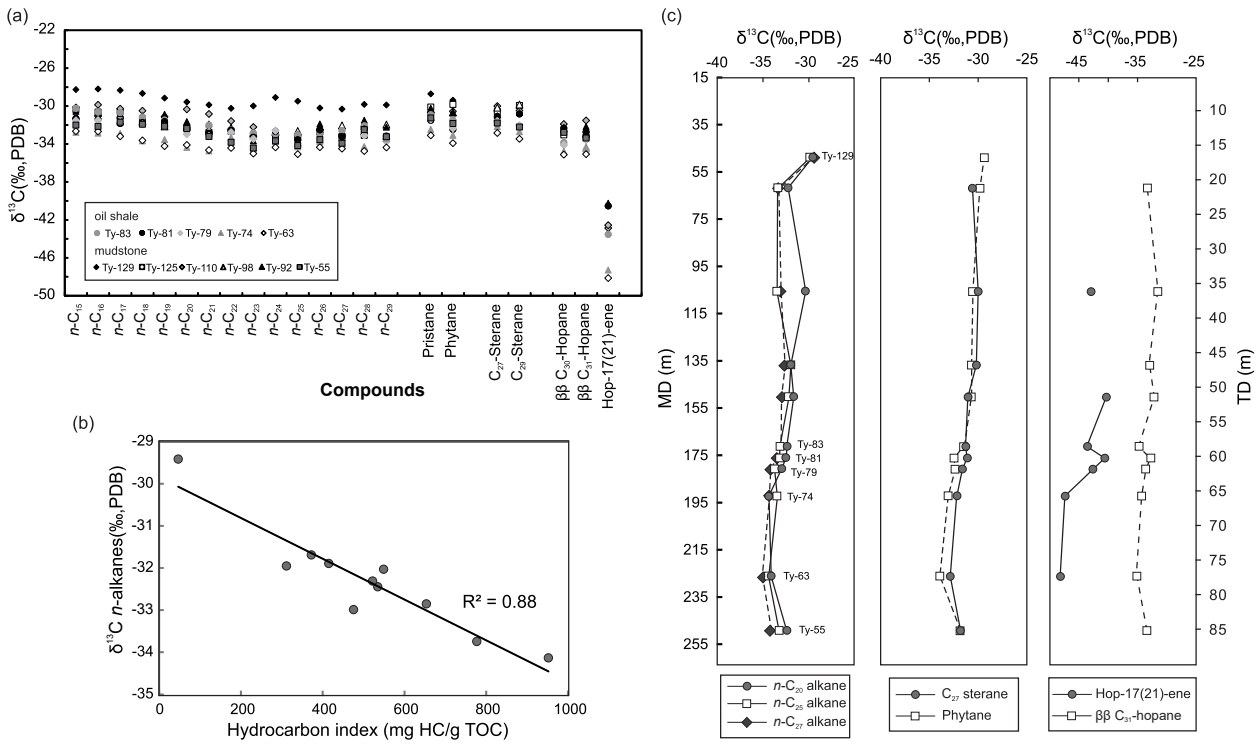

Fig. 10a. Carbon isotopic composition of specific hydrocarbons in saturated hydrocarbon fractions of selected samples from the Shale Member of the Shimengou Formation. (b) Relationship between hydrogen index and $\delta^{13}C$ of n-C_{20}. (c) Variation of $\delta^{13}C$ of n-C_{20}, n-C_{25}, n-C_{27} alkanes, phytane, steranes and hopanes versus depth.

A number of reports of depleted $\delta^{13}C$ values for C_{27}-C_{30}hopanes and hopenes in sediments have been published, and in each case an origin from bacteria utilizing methane as a carbon source (i.e. methylotrophic bacteria or methanotrophs) has been proposed (Freeman *et al.*, 1990; Köster *et al.*, 1998; Aichner *et al.*, 2010; Volkman *et al.*, 2015). The strongly depleted $\delta^{13}C$ values of hop-17(21)-ene in the oil shales (avg. -44.4 ‰) and mudstones (avg. -41.6 ‰) indicates that production by methane-oxidizing bacteria (methanotrophs) also occurred in the Shimengou Lake. Unfortunately, aryl isoprenoids and

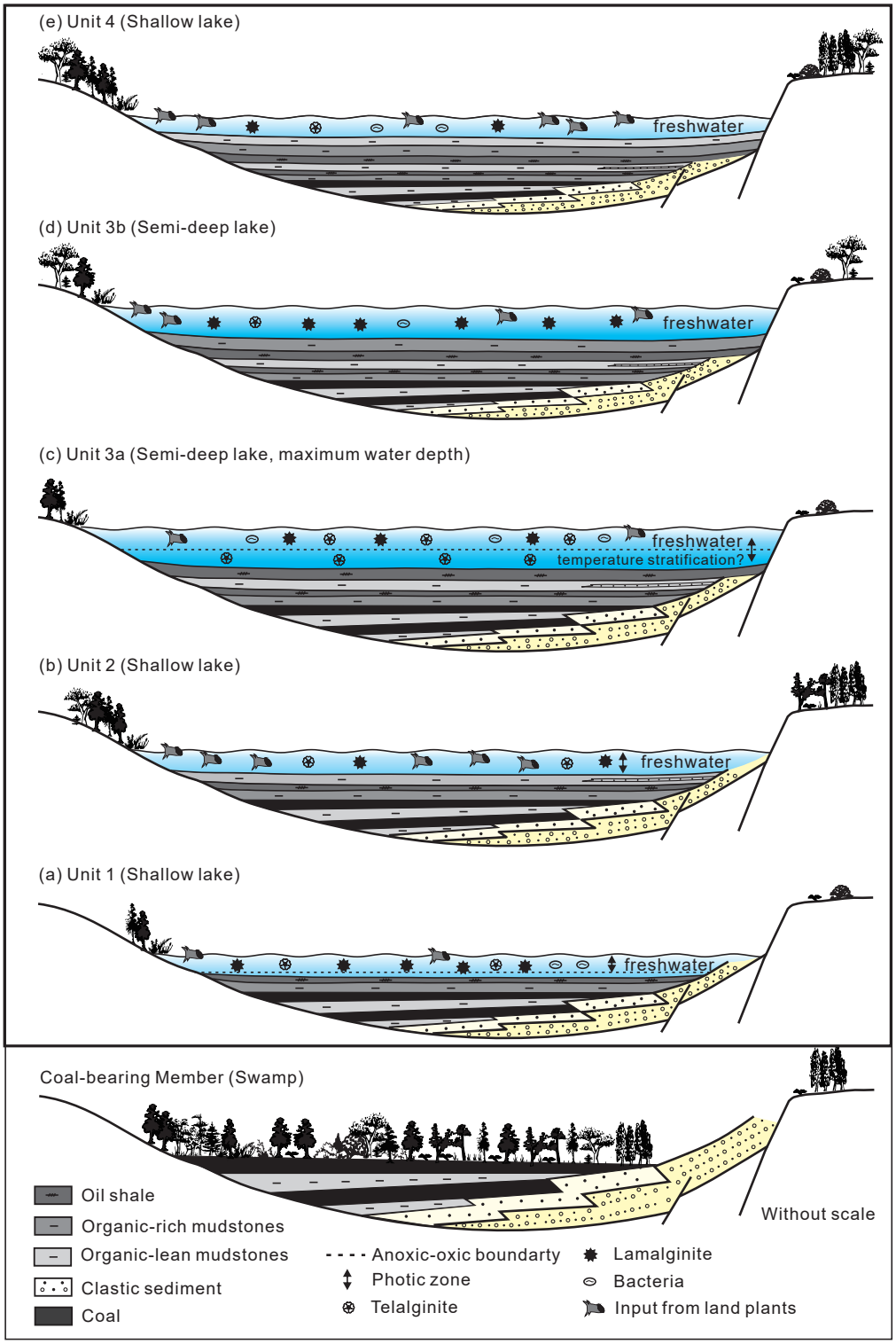

Fig. 11. Cartoon illustrating the depositional environment of the Shale Member and the underlying coal-bearing member of the Shimengou Formation.

β-carotane are present in insufficient concentrations for C-isotope analysis.

A negative correlation between $\delta^{13}C$ of *n*-alkanes and HI is observed (Fig. 10b), and lower $\delta^{13}C$ values are obtained from the oil shale samples (Ty-83-Ty-63) than the mudstone samples (Fig. 10c). Enhanced primary productivity in the oil shale-bearing units, as indicated by high TOC and high concentration of steroids, lead to anoxic bottom water conditions, reflected by the preservation of β-carotane. In such environments, the accumulation of dissolved CO_2 in the water column, originating from the degradation of organic matter (during sulphate reduction or methane oxidation), is possible. This process is known as "CO_2 recycling" of degradation products (Imbus *et al.*, 1992; Bechtel *et al.*, 2012). Subsequent incorporation of this CO_2 into

the biomass by photosynthetic organisms results in isotopically-depleted $\delta^{13}C$ values of the organic matter preserved in the sediments (Lewan, 1986; Fogel *et al.*, 1988; Frimmel *et al.*, 2004).

DISCUSSION

Maturity

The average T_{max} value (433°C), as well as low 22S/(22S+22R) C_{31} hopanes ratios (0.1–0.3), far below the equilibrium value of 0.6 (Mackenzie *et al.*, 1982), indicate that the organic matter is immature. This is supported by a dominance of 5α, 14α, 17α (H) steranes, over 5β, 14α, 17α (H) isomers in the C_{27}–C_{29} range (Fig. 7). Hence, maturity effects have not been considered in the following interpretations.

Palaeoenvironmental reconstruction and organic matter accumulation

The Middle Jurassic coal and oil-shale bearing succession in the northern Qaidam Basin was deposited during a period of continuous rifting (Cao *et al.*, 2005; Lu *et al.*, 2014). In the Saishiteng Depression, rifting commenced in the Middle Jurassic contemporaneous with the formation of a number of other depression in the northern Qaidam Basin (Li *et al.*, 2016). Cartoons illustrating the depositional settings of the four units of the Shale Member of the Shimengou Formation are shown in Fig. 11. A schematic sketch of the depositional environment of the upper part of the Coal-bearing Member of the Shimengou Formation in a low-lying mire, indicated by the accumulation of coal with high ash yields (ca. 24.0 wt.%), is presented at the bottom of Fig. 11 and corresponds to the period before the Shale Member was deposited.

Low sulphur contents and high TOC/S ratios (e.g. Berner, 1984) indicate that freshwater environments prevailed during deposition of the Shale Member (Figs 3d,e).

Unit 1 (shallow lake)

The onset of dark grey mudstone deposition occurred during drowning of a low-lying mire resulting in the formation of a shallow lake (Fig. 11a), and was probably associated with rapid basement subsidence. The high TOC contents and HI values in Unit 1 of the Shale Member indicate a decrease in the input of land plant material after the deposition the underlying Coal-bearing Member (Fig. 3b,c). Alginite (Fig. 6a; lamalgnite, telalginite) is the most frequent maceral and shows an upwards increasing trend. Hopanoids occur in high amounts (89–518 mg/g TOC; Fig. 6d) and reach a maximum in the oil shale Layer 1, indicating an increased contribution of bacterial biomass. The presence of aryl isoprenoids, β-isorenieratane, and β-carotane, as well as strongly depleted $\delta^{13}C$ values of hop-17(21)-ene in the oil shale Layer 1 in the uppermost part (Fig. 6f), indicates the relative contribution of green sulphur bacteria and/or purple non-sulphur bacteria, cyanobacteria and methylotrophic bacteria in the water column. These results suggest an environment with high bioproductivity. The presence of minor diterpenoids and sequiterpenoids (Fig. 6e) suggests that the contribution of terrigenous organic matter is low and dominated by conifers rather than angiosperms.

The presence of C_{14}, C_{16} and C_{19} aryl isoprenoids in the uppermost part of Unit 1 points to photic zone anoxia. The upward decrease of Pr/Ph ratios (Fig. 6c) indicates increasing oxygen depletion and excellent preservation conditions.

Unit 2 (shallow lake)

Deposition of greenish-grey and grey mudstones intercalated with thin siltstones indicates that a shallow lake environment continued during deposition of Unit 2 (Fig. 11b). Low Pr/Ph ratios (0.3–0.5; Fig. 6c) and low amounts of aryl isoprenoids are evidence for the establishment of anoxic conditions in the bottom water of the lake. As β-isorenieratane could not be identified in the sediments of this unit, the origin of aryl isoprenoids from β-carotane could not be excluded (Koopmans *et al.*, 1996) and aryl isoprenoids cannot be unequivocally considered as indicators for photic zone anoxia. Despite the excellent preservation conditions in the anoxic environment, the total amount of organic matter is low (0.6–1.9 wt.% TOC). Moreover, the organic matter is dominated by land plant-derived macerals (Fig. 6a; vitrinite, inertinite). This suggests a strong decrease in the production of lacustrine organic matter. Interestingly, the dominance of land plant material is not reflected by the distribution of *n*-alkanes (Fig. 6b) or sterane patterns (Fig. 9). In addition to a decrease in aquatic bioproductivity, dilution by mineral matter also probably contributed to the low TOC contents.

Unit 3 (semi-deep lake)

The lower part of Unit 3 (3a) includes oil shale layers 2 and 3 with a total thickness of 7 m, as well as organic matter-rich mudstones (oil yield < 3.5 wt.%, Fig. 6a).

Deposition of the lower oil shale Layer 2 corresponds to deepening of the Shimengou Lake, resulting in maximum water levels. High TOC contents (4.8–10.7 wt.%) (Fig. 3b) and HI values (549–815 mg HC/g TOC, Fig. 4) correspond to the presence of abundant Type I to II kerogen. This is consistent with the predominance of abundant telalginite, similar to the Huadian oil shales (Xie *et al.*, 2014) in which the presence of common *Botryococcus* resulted in high HI values. High concentrations of steroids and hopanoids (Fig. 6d) indicate high bioproductivity and bacterial

Table 4. Calculation of the source potential index (SPI) for Units 1-4 in the Shale Member of the Shimengou Formation.

	Thickness (m)	S1+S2 (mg HC/g TOC)	Density (g/cm³)	SPI (t HC/m³)
Unit 4 (net)	5	7.32	2.11	0.08
Unit 3b	34	19.22	2.09	1.37
Unit 3a	14	41.86	1.93	1.13
Unit 2 (net)	2	3.88	2.19	0.02
Unit 1	14	25.55	2.05	0.73

activity leading to water-column stratification and an anoxic depositional environment, as verified by the presence of β-carotane (Fig. 6f). (Fig. 11c). High contents of carbonate minerals indicate a carbonate-rich environment.

In the upper oil shale Layer 3, telalginite occurs in similar amounts to lamalginite. Moreover, a subtle increase in terrigenous macerals and conifer-derived biomarkers indicate an increased input of terrigenous organic matter. Consequently, HI values are slightly lower than that in the underlying organic matter-rich rocks and classifies the organic matter as Type II kerogen (Fig. 4). Less oxygen-deficient conditions are indicated by increasing Pr/Ph ratios (Fig. 6c) and the disappearance of aryl isoprenoids (Fig. 6f).

In general, organic matter-rich mudstones overlying oil shale layer 3 contain higher percentages of lamalginite than the oil shale layers (Fig. 6a), but TOC and HI values remain high. A decrease in Pr/Ph ratios (Fig. 6c) indicates a return to strictly anoxic conditions. The decrease in concentrations of hopanoids (Fig. 6d) indicates minor bacterial biomass. Low contents of carbonate minerals suggest a largely carbonate-free environment.

Mudstones deposited the upper part of Unit 3 (3b) show moderate TOC contents and HI values (Type II kerogen). The vertical TOC, HI and S profiles indicate a stable semi-deep lake environment (water depths between a few tens of metres and 150m) (Fig. 11d). Organic matter is dominated by lamalginite, but land plant-derived macerals (inertinite, vitrinite, minor sporinite) are more abundant than in Unit 3a (Fig. 6a). Relatively high sulphur contents and gradually decreasing TOC/S ratios in the lower part of Unit 3b (53–43 m TD) may indicate a trend towards slightly increased salinity. High contents of carbonate minerals in the uppermost part of Unit 3b (Fig. 3f) and gradually decreasing TOC (Fig. 3b) and HI values (Fig. 3c) suggest the dilution of organic matter by carbonate minerals.

Unit 4 (shallow lake)

Unit 4 includes grey mudstones intercalated with green muddy siltstones, corresponding to a transition to a shallow lake environment (with depths up to a few tens of metres) (Fig. 11e). The Middle Jurassic climate changed from warm-humid to hot-arid during deposition of the uppermost part of the Shimengou Formation (Yang *et al.*, 2007). This suggests that the shallowing of the Shimengou Lake may have been controlled by climatic changes. TOC contents, HI values (Type II to III kerogen) and percentages of alginite macerals are typically low in Unit 4, although low Pr/Ph ratios indicate an anoxic environment with good preservation conditions during deposition of the grey mudstones. Consequently, the relatively low TOC contents are interpreted to indicate varying but typically low aquatic productivity, similar to that in Unit 2.

Thus, the studied succession of the Middle Jurassic Shimengou Formation in the northern Qaidam Basin is characterised by an upward deepening trend (uppermost Coal-bearing Member to oil shale layer in Unit 3a), followed by a shallowing trend (Unit 3a to Unit 4), typical for many other fault-controlled rift basins.

Hydrocarbon potential

Based on the nomenclature of Peters (1986), TOC and Rock-Eval data are used here to evaluate source rock properties in the Shale Member of the Shimengou Formation. Most of the samples from organic-rich Units 1 and 3 contain Type I and II kerogen and have good to very good hydrocarbon generating potential (Fig. 12). In contrast, samples from Units 2 and 4 have (very) poor to fair potential, and only a few samples from the upper part of Unit 4 are characterized by a good potential (Fig. 12). This result are consistent with the data in the adjacent Yuqia area (Hou *et al.*, 2017).

The Source Potential Index, SPI = $(S_1+S_2)*h*\rho$ /1000, where h is thickness and ρ is bulk density (Demaison and Huizinga, 1994) is used to quantify the amount of hydrocarbons which can be generated beneath a 1 m² surface area, and has been calculated for each unit (Table 4). Following Demaison and Huizinga (*ibid.*), only intervals with S_1+S_2 values exceeding 2.0 mg HC/g TOC have been taken into

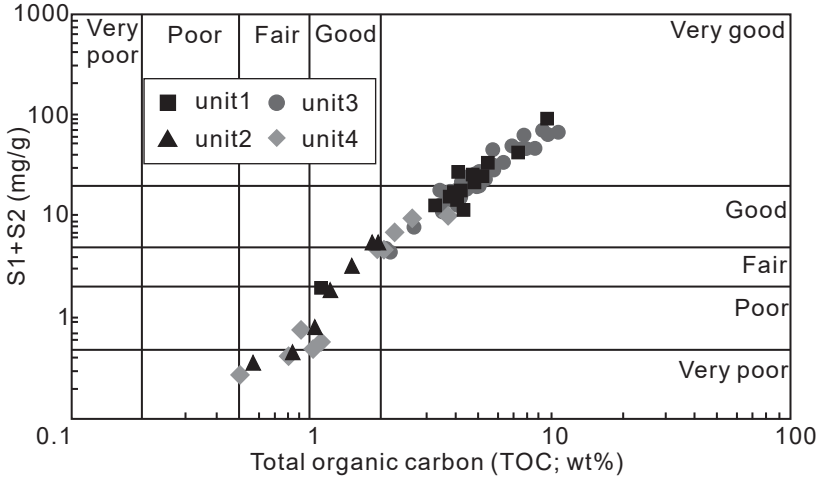

Fig. 12. Plot of generative potential Rock-Eval (S_1+S_2) versus TOC for the four units of the Shale Member of the Shimengou Formation.

account. Considering true thickness values and the average density of 20 samples (1.93–2.19 g/cm³), the SPI in the organic-rich Units 1 and 3 is determined to be 3.2 t HC/m², and the contribution of organic matter-rich intervals in Units 2 and 4 is minor (~0.1 t HC/m²). These results indicate that varying primary aquatic productivity, terrigenous organic matter input, and dilution by minerals are the key factors determining the source rock potential for conventional hydrocarbons.

The oil yields of 1 m core sections from the most organic matter-rich intervals range from 1.0–7.1 wt.% (Fig. 3a) and show that oil shales (>3.5 wt.%) are restricted to the upper part of Unit 1 and Unit 3a. Oil yields ranging from 3.6 to 7.1 wt% classify these intervals as low-medium quality oil shales following Liu *et al.* (2009). Compared with oil shales from Eocene fault-related coal-bearing basins in NE China such as the Fushun and Huadian Basins (Strobl *et al.*, 2014, 2015), the relatively low quality of the Tuanyushan oil shales may be related to the lower organic productivity as reflected by the lower TOC contents.

The data are of regional significance for petroleum exploration, with respect to the area of the northern Qaidam Basin of about 34,000 km² covered by the source rocks. The outlined key factors controlling the abundance and type of organic matter in the Shimengou Formation may contribute to the identification of future exploration targets.

CONCLUSIONS

The Middle Jurassic Shale Member of the Shimengou Formation in the northern Qaidam Basin has TOC contents varying between 0.6 and 10.7 wt.% (avg. 4.3 wt.%). HI values range from 43 to 952 mg HC/g TOC (avg. 424 mg HC/g TOC). Variations of these bulk geochemical data versus depth outline four units: two organic-rich units (Units 1 and 3) with relatively high TOC contents and Type I-II kerogen; and two organic-lean units (Units 2 and 4) with low TOC contents and Type II-III kerogen.

Bulk geochemical data and biomarkers indicate that the oil shale-bearing intervals in the Shimengou Formation were deposited in an anoxic freshwater lake which originated after drowning of a precursor mire. The evolution of the Shimengou Lake reflects a continuous deepening upward-trend followed by a shallowing trend, and can be divided into four stages.:

The lower part of the sequence (Unit 1) contains thick organic-rich mudstones interbedded with a thin oil shale layer, and represents the first tectonically controlled flooding of the Shimengou Lake. During this time interval, algae (e.g. *Pila*), green sulphur bacteria and/or purple non-sulphur bacteria, cyanobacteria and methylotrophic bacteria were the dominant primary producers of organic matter. Photic zone anoxia is indicated by the occurrence of β-isorenieratane together with aryl isoprenoids.

Green-grey and grey mudstones intercalated with thin siltstones show that a shallow lake environment continued during deposition of Unit 2. The low TOC contents in this unit result from low productivity of lacustrine organisms (algae and bacteria) and dilution by detrital minerals.

The oil shale layers in the lower part of Unit 3 (3a) were deposited when water depths reached a maximum. The organic matter in these oil shales is dominated by telalginite and bacteria, resulting in Type I and II kerogen. Photic zone anoxia supported by water column stratification in a semi-deep lake controlled organic matter preservation. Decay-resistant plants (e.g. conifers) contributed to organic matter deposition. The vertical changes in TOC, HI and S in the upper part of Unit 3 (3b) indicate a stable semi-deep lake environment. Organic matter was dominated by

lamalginite. The presence of higher amounts of land plant material than in the underlying units resulted in lower HI values (Type II kerogen).

The uppermost part of the Shale Member (Unit 4) is characterized by grey mudstones interbedded with green muddy siltstones, reflecting a transition to a shallow lake. Similar to Unit 2, the low TOC contents may be related to the low productivity of aquatic organisms and dilution by detrital minerals.

These data indicate that bioproductivity and organic matter dilution are the key factors which controlled the abundance and types of organic matter in the Middle Jurassic Shimengou Formation.

Based on TOC and Rock-Eval pyrolysis data, oil shales and organic-rich mudstones in Units 1 and 3 are excellent source rocks for conventional oil, with a Source Potential Index of 3.2 t HC/m^2.

ACKNOWLEDGEMENTS

We thank Li Feng and Xu Yinbo from the Survey Center of Oil & Gas Resources of the China Geological Survey for their support during core inspection and sample collection. This study was financially supported by the China Geological Survey (DD20160188-01). The bulk geochemical data were measured at the Key Laboratory for Oil Shale and Paragenetic Energy Minerals at Jilin University (China), and organic petrographic, biomarker and compound specific carbon isotope data were measured at the Department of Applied Geosciences and Geophysics at Montan Universität Leoben (Austria). Qingtao Meng thanks the Program of Study Abroad for Young Scholars sponsored by the China Scholarship Council (CSC) (No.201606175105) for a 12 month scholarship at Montan University Leoben, Austria. The article benefited from critical remarks by Willi Püttmann (*Goethe-University Frankfurt am Main*) and an anonymous reviewer.

REFERENCES

AICHNER, B., WILKES, H., HERZSCHUH, U., MISCHKE, S. and ZHANG, C.J., 2010. Biomarker and compound-specific $\delta^{13}C$ evidence for changing environmental conditions and carbon limitation at Lake Koucha, eastern Tibetan Plateau. *Journal of Paleolimnology*, **43**, 873-899.

BAO, JING, YADONG WANG, CHUNHUI SONG, YING FENG, CHUNHUA HU, SIRUI ZHONG and JIWEI YANG, 2017. Cenozoic sediment flux in the Qaidam Basin, northern Tibetan Plateau, and implications with regional tectonics and climate. *Global and Planetary Change* **155**, 56-69.

BAO, Y., WEI, C.T., PENG, D.H., JIANG, B. and WANG, C.Y., 2013. Quantitative identification of coal-type gas and oil-type gas in source-mixed gas at the northern margin of Qaidam Basin. *International Journal of Mining Science and Technology*, **23**(3), 435-439.

BECHTEL, A., JIA, J.L., STROBL, S. A., SACHSENHOFER, R. F., LIU, Z.J., GRATZER, R. and PÜTTMANN, W. 2012. Palaeoenvironmental conditions during deposition of the Upper Cretaceous oil shale sequences in the Songliao Basin (NE China): implications from geochemical analysis. *Organic Geochemistry*, **46**, 76-95.

BECHTEL, A., OBERAUER, K., KOSTIĆ, A., GRATZER, R., MILISAVLJEVIĆ, V., ALEKSIĆ, N., STOJANOVIĆ, K., GROß, D. and SACHSENHOFER, R.F., 2018. Depositional environment and hydrocarbon potential of the Lower Miocene oil shale deposit in the Aleksinac Basin (Serbia). *Organic Geochemistry*, **115**, 93-112.

BERNER, R.A., 1984. Sedimentary pyrite formation: an update. *Geochimica et Cosmochimica Acta,* **48**, 605-615.

BRAY, E.E. and EVANS, E.D., 1961. Distribution of n-paraffins as a clue to recognition of source beds. *Geochimica et Cosmochimica Acta*, **22**, 2-15.

BROCKS, J.J. and SCHAEFFER, P., 2008. Okenane, a biomarker for purple sulfur bacteria (Chromatiacaceae), and other new carotenoid derivatives from the 1640 Ma Barney Creek Formation. *Geochimica et Cosmochimica Acta,* **72,** 1396-1414.

CAO, G.Q., CHEN, S.Y., XU, F.Y., PENG, D.H. and YU, W.F., 2005. Ceno-Mesozoic sedimentary and tectonic evolution in the western Qaidam basin. *Geology in China*, **1**, 33-40 (in Chinese with English abstract).

CAO, J., HU, K., WANG, K., BIAN, L.Z., LIU, Y.T., YANG, S.Y., WANG, L.Q. and CHEN, Y., 2008. Possible origin of 25-norhopanes in Jurassic organic-poor mudstones from the northern Qaidam Basin (NW China). *Organic Geochemistry*, **39**, 1058-1065.

CHEN, X.H., GEORGE, G., YIN, A., LI, L. and JIANG, R.B., 2012. Paleozoic and Mesozoic basement magmatisms of Eastern Qaidam Basin, northern Qinghai–Tibet Plateau: LA-ICP-MS zircon U-Pb geochronology and its geological significance. *Acta Geologica Sinica (English Edition)*, **86**(2), 350-369.

COLLISTER, J.W., RIELEY, G., STERN, B., EGLINTON, G. and FRY, B., 1994. Compound-specific $\delta^{13}C$ analysis of leaf lipids from plants with differing carbon dioxide metabolism. *Organic Geochemistry*, **21**, 619-627.

COPLEN, T. B., 2011. Guidelines and recommended terms for expression of stable-isotope ratio and gas-ratio measurement results. *Rapid Communications in Mass Spectrometry*, **25**, 2538-2560.

CRANWELL, P.A., 1977. Organic geochemistry of Cam Loch (Sutherland) sediments. *Chemical Geology*, **20**, 205-221.

DAI, J.S., YE, X.S., TANG, L.J., JIN, Z.J., SHAO, W.B., HU, Y., and ZHANG, B.S. 2003. Tectonic units and oil-gas potential of the Qaidam Basin. *Chinese Journal of Geology* **38**(3), 291-296 (in Chinese with English abstract).

DEMAISON, G. and HUIZINGA, B.J., 1994. Genetic classification of petroleum systems using three factors: charge, migration, and entrapment. In: Magoon, L.B., Dow, W.G. (Eds.), The Petroleum System, From Source to Trap. *AAPG Memoir* **60,** 3-24.

DIDYK, B.M., SIMONEIT, B.R.T., BRASSELL, S.C. and EGLINTON, G., 1978. Organic geochemical indicators of palaeoenvironmental conditions of sedimentation. *Nature,* 272, 216-222.

EGLINTON, G. and HAMILTON, R.J., 1967. Leaf epicuticular waxes. *Science*, **156**, 1322-1335.

ESPITALIÉ, J., MARQUIS, F. and BARSONY, I., 1984. Geochemical Logging. *Analytical Pyrolysis*, **184**, 276-304.

FICKEN, K.J., LI, B., SWAIN, D.L. and EGLINTON, G., 2000. An n-alkane proxy for the sedimentary input of submerged/floating freshwater aquatic macrophytes. *Organic Geochemistry*, **31**, 745-749.

FOGEL, M.L., VELINSKY, D.J., CIFUENTES, L.A., PENNOCK, J.R. and SHARP, J.H., 1988. Biogeochemical processes affecting the stable carbon isotopic composition of particulate carbon in the Delaware Estuary. Carnegie Institute Washington Annual Report Directory 1988, pp. 107-113.

FREEMAN, K. H., HAYES, J. M., TRENDEL, J. M. and ALBRECHT, P., 1990. Evidence from carbon isotope measurements for diverse origins of sedimentary hydrocarbons. *Nature,* 343, 254.

FRIMMEL, A., OSCHMANN, W. and SCHWARK, L., 2004. Chemostratigraphy of the Posidonia Shale, SW Germany I. Influence of sea-level variation on organic facies evolution. *Chemical Geology*, 206, 199-230.

GOOSSENS, H., DE LEEUW, J.W., SCHENCK, P.A. and BRASSELL, S.C., 1984. Tocopherols as likely precursors of pristane in ancient sediments and crude oils. *Nature*, **312,** 440-442.

GRANTHAM, P. J. and WAKEFIELD, L. L., 1988. Variations in the sterane carbon number distributions of marine source rock derived crude oils through geological time. *Organic Geochemistry*, **12,** 61-73.

HANSON, A.D., RITTS, B.D., ZINNIKER, D., MOLDOWAN, J.M. and BIFFI, U., 2001. Upper Oligocene lacustrine source rocks and petroleum systems of the northern Qaidam basin, northwest China. *AAPG Bulletin*, **85,** 601-619.

HOU, H.H., SHAO, L.YY., LI, Y.H., LI, Z., WANG, S., ZHANG, W.L. and WANG, X.T., 2017a. Influence of coal petrology on methane adsorption capacity of the Middle Jurassic coal in the Yuqia Coalfield, northern Qaidam Basin, *China. Journal of Petroleum Science and Engineering*, **149**, 218-227.

HOU, H.H., SHAO, L., LI, Y., LU, J., LI, Z., WANG, S., ZHANG, W. and WEN, H., 2017b. Geochemistry, reservoir characterization and hydrocarbon generation potential of lacustrine shales: A case of YQ-1 well in the Yuqia Coalfield, northern Qaidam Basin, NW China. *Marine and Petroleum Geology*, **88**, 458-471.

HUNT, J.M., 1996. Petroleum Geochemistry and Geology. Freeman and Company.

HUSSLER, G., CONNAN, J. and ALBRECHT, P., 1984. Novel families of tetra-and hexacyclic aromatic hopanoids predominant in carbonate rocks and crude oils. *Organic Geochemistry*, **6**, 39-49.

IMBUS, S.W., MACKO, S.A., ELMORE, R.D. and ENGEL, M.H., 1992. Stable isotopes (C, S, N) and molecular studies on the Precambrian Nonesuch Shale (Wisconsin, Michigan, USA): evidence for differential preservation rates, depositional environment and hydrothermal influence. *Chemical Geology,* **101**, 255–281.

KODNER, R.B., SUMMONS, R.E., PEARSON, A., KING, N. and KNOLL, A.H., 2008. Sterols in a unicellular relative to metazoans. *Proc. Natl. Acad. Sci. USA*, **105**, 9897-9902.

KOOPMANS, M.P., SCHOUTEN, S., KOHNEN, M.E.I. and SINNINGHE DAMSTÉ, J.S., 1996. Restricted utility of aryl isoprenoids as indicators for photic zone anoxia. *Geochimica et Cosmochimica Acta*, **60**, 4873–4876.

KÖSTER, J., ROSPONDEK, M., SCHOUTEN, S., KOTARBA, M., ZUBRZYCKI, A. and SINNINGHE DAMSTÉ, J.S., 1998. Biomarker geochemistry of a foreland basin: the Oligocene Menilite Formation in the Flysch Carpathians of Southeast Poland. *Organic Geochemistry,* **29**, 649-669.

LANGFORD, F.F. and BLANC-VALLERON, M., 1990. Interpreting Rock-Eval Pyrolysis data using graphs of pyrolizable hydrocarbons vs. total organic carbon. *AAPG Bulletin*, **74**(6), 799-804.

LEWAN, M.D., 1986. Stable carbon isotopes of amorphous kerogens from Phanerozoic sedimentary rocks. *Geochimica et Cosmochimica Acta*, **50,** 1583-1591.

LI, M., SHAO, L.Y., LU, J., SPIRO, B. and WEN, H. J., LI, Y.H., 2014. Sequence stratigraphy and paleogeography of the Middle Jurassic coal measures in the Yuqia coalfield, northern Qaidam Basin, northwestern China. *AAPG Bulletin,* **98,** 2531-2550.

Li, M., 2014. Sedimentology and shale gas accumulation of the Jurassic in the northern Qaidam Basin. Doctoral thesis, China University of Mining & Technology, Beijing, p. 83.

LI, M., SHAO, L.Y., LIU, L., LU, J., SPIRO, B., WEN, H. J. and LI, Y. H., 2016. Lacustrine basin evolution and coal accumulation of the Middle Jurassic in the Saishiteng coalfield, northern Qaidam Basin, China. *Journal of Palaeogeography* **5**(3), 205-220.

LI, X., WANG, D.L., LIU, B.Q., REN, C.L., GUO, J.Y., SU, X.F. and WANG, J., 2008. Simulation experiment on hydrocarbon generating potential of various source rocks on the northern margin of the Qaidam Basin, Qinghai, *China. Chinese Journal of Geochemistry,* **27**(4), 412-419.

LIU, Z.J., YANG, H.L., DONG, Q.S., ZHU, J.W., GUO, W., YE, S.Q., LIU, R., MENG, Q.T., ZHANG, H.L. and GAN, S.C., 2009. Oil Shale in China. Petroleum Industry Press, Beijing, pp. 38-116 (in Chinese with English Abstract).

LU, J., SHAO, L.Y., JU, Q., LIU, T.J., WEN, H.J., LI, Y.H., ZHANG, F.D. and GAO, D.Y. 2009. Coal petrography variation in the sequence stratigraphic frame of the Jurassic coal measures of Dameigou mine area in Northern Qaidam Basin. *Coal geology and exploration,* **37,** 9-14 (in Chinese with English abstract).

LU, H.J., WANG, E.C. and MENG, K., 2014. Paleomagnetism and anisotropy of magnetic susceptibility of the Tertiary Janggalsay section (southeast Tarim basin): implications for Miocene tectonic evolution of the Altyn Tagh range. *Tectonophysics* **618**, 67-78.

MACKENZIE, A. S., BRASSELL, S. C., EGLINTON, G. and MAXWELL, J. R., 1982. Chemical fossils: the geological fate of steroids. *Science,* **217**, 491-504.

OTTO, A., WALTHER, H. and PÜTTMANN, W., 1997. Sesqui- and diterpenoid biomarkers in Taxodium-rich Oligocene oxbow lake clays Weisselster basin Germany. *Org. Geochem.*, **26**, 105-115.

OTTO, A. and WILDE, V., 2001. Sesqui-, di-, and triterpenoids as chemosystematic markers in extant conifers-a review. *Bot. Rev.*, **67**, 141-238.

OURISSON, G., ALBRECHT, P. and ROHMER, M., 1979. The hopanoids: palaeochemistry and biochemistry of a group of natural products. *Pure and Applied Chemistry,* **51**(4), 709-729.

PETERS, K. E., 1986. Guidelines for evaluating petroleum source rock using programmed pyrolysis. *AAPG Bulletin*, **70**, 318-329.

PETERS, K. E., MOLDOWAN, J. M., DRISCOLE, A. R. and DEMAISON, G. J., 1989. Origin of Beatrice oil by co-sourcing from Devonian and Middle Jurassic source rocks, inner Moray Firth, United Kingdom. *AAPG Bulletin*, **73**, 454-471.

PETERS, K. E., SNEDDEN, J. W., SULAEMAN, A., SARG, J. F. and ENRICO, R. J., 2000. A new geochemical-sequence stratigraphic model for the Mahakam Delta and Makassar Slope, Kalimantan, Indonesia. *AAPG Bulletin*, **84**, 12-44.

PETERS, K.E., WALTERS, C.C. and MOLDOWAN, J.M., 2005. The Biomarker Guide, Biomarkers and Isotopes in Petroleum Exploration and Earth History, vols. 1 and 2. Cambridge University Press, New York, NY.

RADKE, M., WILLSCH, H. and WELTE, D.H., 1980. Preparative hydrocarbon group type determination by automated medium pressure liquid chromatography. *Anal. Chem.*, **52,** 406–411.

REPETA, D.J. 1989. Carotenoid diagenesis in recent marine sediments – II. Degradation of fucoxanthin to loliolide. *Geochimica et Cosmochimica Acta*, **53**, 699-707.

REPETA, D.J. and GAGOSIAN, R.B., 1987. Carotenoid diagenesis in recent marine sediments – I. The Peru continental shelf (15°S, 75°W). *Geochimica et Cosmochimica Acta,* **51**, 1001-1009.

RITTS, B.D., HANSON, A.D., ZINNIKER, D. and MOLDOWAN, J.M., 1999. Lower–Middle Jurassic nonmarine source rocks and petroleum systems of the Northern Qaidam Basin, Northwest China. *AAPG Bulletin*, **83**, 1980-2005.

ROHMER, M., BISSERET, P. and NEUNLIST, S., 1992. The hopanoids, prokaryotic triterpenoids and precursors of ubiquitous molecular fossils. *Biological Markers in Sediments*

and Petroleum, **54**, 1-17.

SCHOUTEN, S., SCHOELL, M., SINNIGHE DAMSTÉ, J.S., SUMMONS, R.E. and DE LEEUW, J.W., 1998. Molecular biogeochemistry of Monterey sediments (Naples Beach, USA). II: carbon isotopic composition of free and sulphur-bound carbon skeletons. In: Isaacs, C.M., Rullkötter, J. (Eds), The Monterey Formation: From Rock to Molecules. Columbia University Press, New York, pp. 175-188.

SHAO, L.Y., LI, M., LI, Y.H., ZHANG, Y.P., LU, J., ZHANG, W.L., TIAN, Z. and WEN, H.J. 2014. Geological characteristics and controlling factors of shale gas in the Jurassic of the northern Qaidam Basin. *Earth Science Frontiers* **21**(4), 311-322 (in Chinese with English abstract).

STROBL, S.A., SACHSENHOFER, R.F., BECHTEL, A., GRATZER, R., GROSS, D., BOKHARI, S.N., LIU, R., LIU, Z.J., MENG, Q.T. and SUN, P.C., 2014. Depositional environment of oil shale within the Eocene Jijuntun Formation in the Fushun Basin (NE China). *Mar. Pet. Geol.*, **56**, 166-183.

STROBL, S.A., SACHSENHOFER, R.F., BECHTEL, A., MENG, Q.T. and SUN, P.C., 2015. Deposition of coal and oil shale in NE China: the Eocene Huadian Basin compared to the coeval Fushun Basin. *Mar. Pet. Geol.*, **64**, 347-362.

SUMMONS, R.E. and POWELL, T.G., 1987. Identification of aryl isoprenoids in source rocks and crude oils: biological markers for the green sulphur bacteria. *Geochimica et Cosmochimica Acta*, **51**, 557-566.

TAYLOR, H., TEICHMÜLLER, M., DAVIS, A., DIESSEL, C.F.K., LITTKE, R. and ROBERT, P., 1998. Organic Petrology. Borntraeger, Berlin-Stuttgart, 704.

TISSOT, B.T. and WELTE, D.H., 1984. Petroleum Formation and Occurence, 2nd ed., Springer Verlag, Berlin.

VOLKMAN, J.K. and MAXWELL, J.R., 1986. Acyclic isoprenoids as biological markers. In: Johns, R.B. (Ed.), Biological Markers in the Sedimentary Record. Elsevier, Amsterdam, pp. 1-42.

VOLKMAN, J. K., BARRETT, S. M., BLACKBURN, S. I., MANSOUR, M. P., SIKES, E. L. and GELIN, F. 1998. Microalgal biomarkers: a review of recent research developments. *Organic Geochemistry,* **29**, 1163-1179.

VOLKMAN, J.K., ZHANG, Z.Z., XIE, X.M., QIN, J.Z. and BORJIGIN, T., 2015. Biomarker evidence for Botryococcus and a methane cycle in the Huadian oil shale, NE China. *Organic Geochemistry,* **78**, 121-134.

WANG, T.T., YANG, S.Y., DUAN, S.S., CHEN, H.T., LIU, H.Z. and CAO, J., 2015. Multi-stage primary and secondary hydrocarbon migration and accumulation in lacustrine Jurassic petroleum systems in the northern Qaidam Basin, NW China. *Marine and Petroleum Geology*, **62**, 90-101.

WANG, Y.D., MOSBRUGGER, V. and ZHANG, H., 2005. Early to Middle Jurassic vegetation and climatic events in the Qaidam Basin, Northwest China. *Palaeogeography, Palaeoclimatology, Palaeoecology,* **224**, 200-216.

XIE, X.M., VOLKMAN, J.K., QIN, J.Z., BORJIGIN, T., BIAN, L.Z. and ZHEN, L.J. 2014. Petrology and Hydrocarbon Potential of Microalgal and Macroalgal Dominated Oil Shales from the Eocene Huadian Formation, NE China . *International Journal of Coal Geology*, **124**, 36-47.

YANG, P., YANG, Y.Q., MA, L.X., DONG, N. and YUAN, X.J. 2007. Evolution of the Jurassic sedimentary environment in northern margin of Qaidam Basin and its significance in petroleum geology. *Petroleum Exploration and Development*, **34** (2), 160-164. (in Chinese with English abstract).

ZHANG, J.X., YANG, J.S., MATTINSON, C.G., XU, Z.Q., MENG, F.C. and SHI, R.D., 2005. Two contrasting eclogite cooling histories, North Qaidam HP/UHP terrane, western China: Petrological and isotopic constraints. *Lithos,* **84**, 51-76.

Appendix 1. Data from elemental analyses, Rock-Eval pyrolysis and organic petrography.
MD: measured depth; TD: true stratigraphic depth; TOC: total organic carbon; HI: hydrogen index; S_2: hydrocarbons generated during Rock-Eval pyrolysis; T_{max}: temperature of maximum hydrocarbon generation; S: sulphur; $Calc_{eq}$: calcite equivalent; Terrig. OM: terrigenous organic matter; Lamalg.: lamalginite; Telalg.: telalginite.

Smaple	MD	TD	TOC	HI (mg/g	S_1	S_2	Tmax	TS	TOC/S	$Calc_{eq}$	Lamalg.	Telalg.	Terrig. OM (vol.%, mmf)		
	(m)	(m)	(wt.%)	TOC)	(mg/g)	(mg/g)	(°C)	(wt.%)	(-)	(wt.%)	(vol.%, mmf)	(vol.%, mmf)	Sporinite	Vitrinite	Inertinite
Unit 4															
TY-138	17.8	6.1	2.0	234	0.07	4.7	430	0.1	19.5	29.3					
TY-137	20.4	7.0	3.7	278	0.13	10.2	427	0.1	31.9	15.83					
TY-136	25.1	8.6	2.2	317	0.09	7.0	432	—	—	—	17	26		35	22
TY-135	29.7	10.1	0.9	77	0.08	0.7	434	0.1	10.0	7.65					
TY-134	34.0	11.6	0.5	51	0.03	0.2	437	0.1	4.6	37.9					
TY-132	38.4	13.1	2.6	364	0.16	9.5	431	0.2	16.2	3.79					
TY-131	40.8	13.9	1.9	256	0.06	4.8	429	0.1	16.8	11.04					
TY-130	44.9	15.3	1.1	51	0.02	0.6	435	0.1	14.5	2.75					
TY-129	48.7	16.6	1.0	47	0.02	0.5	433	0.0	52.1	1.26	0	2		67	32
TY-128	53.6	18.3	0.8	43	0.08	0.3	435	0.1	9.6	9.91					
Unit 3															
TY-127	56.0	19.2	4.1	378	0.15	15.6	431	0.1	43.1	10.50					
TY-126	58.7	20.1	2.1	208	0.12	4.4	428	0.1	22.4	11.33					
TY-125	61.7	21.1	4.2	522	0.15	21.9	436	0.1	33.2	27.29	52	22	1	6	19
TY-124	64.1	21.9	2.7	298	0.07	8.0	426	0.1	19.0	40.29					
TY-123	66.3	22.7	5.1	478	0.13	24.4	431	0.1	47.1	1.58					
TY-122	68.8	23.5	4.0	369	0.08	14.9	431	0.2	25.9	1.87					
TY-121	70.5	24.1	5.0	558	0.10	28.0	437	0.2	29.7	5.62					
TY-120	74.7	25.5	3.6	394	0.08	14.1	432	0.2	18.9	5.17					
TY-119	77.3	26.4	4.6	474	0.11	21.8	432	0.2	27.9	4.25					
TY-118	80.7	27.6	5.0	440	0.14	21.8	433	0.2	32.4	2.40	43	12	2	9	36
TY-117	86.6	29.6	4.6	448	0.13	20.7	433	0.1	41.5	4.34					
TY-116	90.4	30.9	5.4	490	0.13	26.3	435	0.2	25.7	2.62					
TY-115	93.3	31.9	4.0	456	0.09	18.3	438	0.2	17.3	2.46					
TY-114	95.8	32.8	4.9	400	0.10	19.5	435	0.1	50.4	0.50					
TY-113	98.2	33.6	3.7	409	0.11	15.0	437	0.1	40.0	4.28					
TY-112	100.6	34.4	3.4	382	0.27	13.2	434	0.1	38.8	4.75					
TY-111	103.0	35.2	4.7	436	0.13	20.5	437	0.1	53.0	3.97					
TY-110	105.5	36.1	3.5	373	0.09	13.0	439	0.1	38.4	4.54	57	19		5	18
TY-109	109.4	37.4	4.3	428	0.12	18.6	436	0.1	52.7	3.45					
TY-108	113.3	38.7	5.7	513	0.13	29.2	437	0.1	45.9	1.08					
TY-107	115.7	39.6	5.7	583	0.14	33.2	438	0.1	63.4	4.62					
TY-106	118.1	40.4	3.8	477	0.12	18.0	427	0.1	28.3	10.96					
TY-105	120.4	41.2	5.3	450	0.11	23.7	435	0.1	64.8	3.29					
TY-104	123.1	42.1	5.5	527	0.12	29.1	434	0.1	45.2	8.34	41	17		9	32
TY-103	125.2	42.8	4.0	448	0.08	17.9	435	0.2	17.3	3.00					
TY-102	128.1	43.8	4.3	462	0.14	19.7	439	0.2	18.2	2.21					
TY-101	129.8	44.4	3.9	433	0.12	16.7	434	0.1	26.8	3.00					
TY-100	132.5	45.3	4.0	421	0.09	17.0	432	0.3	15.8	2.03					
TY-99	134.2	45.9	4.2	426	0.08	17.9	435	0.2	16.9	32.83					
TY-98	136.7	46.8	3.5	312	0.30	10.9	433	0.1	27.0	2.54	48	21		12	15
TY-97	138.9	47.5	4.5	493	0.11	22.0	434	0.3	17.5	1.96					
TY-96	141.5	48.4	5.0	545	0.11	27.2	433	0.1	40.6	2.79					
TY-95	143.5	49.1	4.1	479	0.10	19.6	433	0.1	30.9	3.17					
TY-94	145.9	49.9	4.1	460	0.12	18.7	432	0.1	29.1	5.17					
TY-93	147.2	50.4	4.8	524	0.10	25.4	435	0.1	33.8	3.71					
TY-92	150.2	51.4	3.8	415	0.09	15.7	434	0.5	7.3	1.83	42	25		6	27
TY-91	152.4	52.1	2.0	235	0.10	4.8	434	0.1	13.8	3.58					
TY-90	155.0	53.0	4.5	554	0.10	25.2	435	0.2	25.2	4.58	51	30		3	16
TY-89	157.3	53.8	7.7	845	0.23	64.8	438	0.1	56.0	4.58					
TY-88	159.5	54.6	5.6	498	0.10	27.9	437	0.2	36.7	3.46	53	28		3	17
TY-87	162.2	55.5	6.2	559	0.14	34.7	433	0.1	55.2	3.92					
TY-86	164.1	56.1	5.3	495	0.10	26.4	434	0.2	33.5	1.96	46	24	1	5	25
TY-85	166.3	56.9	4.1	324	0.08	13.1	430	0.1	27.1	19.42					
TY-84	169.3	57.9	9.7	679	0.65	65.7	437	0.1	87.2	7.25					
TY-83	171.1	58.5	6.3	549	0.28	34.7	433	0.2	30.3	5.12	38	45		2	15
TY-82	173.3	59.3	8.5	561	0.33	47.8	435	0.2	48.7	3.54					
TY-81	176.0	60.2	5.7	535	0.23	30.2	432	0.1	66.3	3.42	51	34		3	12
TY-80	179.1	61.2	7.4	625	0.39	46.5	430	0.3	29.2	22.21					
TY-79	180.7	61.8	10.7	654	0.52	69.7	435	0.5	20.8	0.83	32	49		2	18
TY-78	183.6	62.8	7.9	608	0.35	47.8	433	0.4	20.2	3.21					

Appendix 1 (*cont.*).

TY-77	185.3	63.4	5.7	815	0.54	46.3	431	0.3	21.6	38.87	31	51	6	13
TY-76	187.8	64.2	4.8	553	0.22	26.5	436	0.7	6.5	17.87	26	59	2	14
TY-75	190.0	65.0	6.9	741	0.38	50.8	437	0.5	13.0	23.46				
TY-74	192.1	65.7	9.2	777	1.26	71.4	440	0.3	36.8	35.08	36	49	5	9
TY-73	194.8	66.6	3.5	511	0.22	17.8	430	0.2	21.5	22.42	42	45	1	12
Unit 2														
TY-72	197.1	67.4	1.2	137	0.13	1.6	429	0.1	12.0	6.75	6	0	59	35
TY-71	200.8	68.7	1.8	294	0.05	5.3	423	0.1	23.2	11.67				
TY-70	203.1	69.5	1.0	71	0.03	0.7	434	0.1	13.6	2.33				
TY-69	205.9	70.4	0.8	45	0.05	0.4	431	0.0	25.9	4.62	2	0	59	39
TY-68	208.3	71.2	1.5	206	0.05	3.0	432	0.1	17.7	7.25				
TY-67	210.6	72.0	1.9	276	0.07	5.3	431	0.1	22.6	6.37				
TY-66	213.5	73.0	0.6	52	0.04	0.3	431	0.0	86.9	0.15	2	0	87	11
Unit 1														
TY-65	220.4	75.4	4.1	676	0.20	27.8	434	0.4	11.6	42.46	48	43	1	8
TY-64	222.3	76.0	5.5	611	0.16	33.3	438	0.2	23.7	10.54				
TY-63	226.1	77.3	9.6	952	1.82	91.6	430	0.1	80.5	41.08	44	37	1	17
TY-62	229.4	78.4	1.1	179	0.04	2.0	427	0.2	4.9	7.58				
TY-61	231.5	79.2	7.3	585	0.37	42.7	432	0.2	39.8	9.12				
TY-60	235.1	80.4	4.7	551	0.10	25.8	434	0.0	130.7	9.08				
TY-59	238.6	81.6	4.0	451	0.10	17.9	431	0.2	26.2	6.37				
TY-58	241.9	82.7	4.1	338	0.19	13.7	425	0.1	43.1	5.96	47	29	4	20
TY-57	244.3	83.6	4.8	434	0.27	20.9	436	0.1	49.6	5.17				
TY-56	246.9	84.4	3.3	398	0.09	13.1	433	0.1	31.6	3.54				
TY-55	249.1	85.2	4.8	476	0.14	23.0	435	0.1	34.4	3.79	44	25	5	26
TY-54	251.0	85.9	3.8	406	0.30	15.5	435	0.2	23.0	2.46				
TY-53	253.9	86.8	4.2	434	0.11	18.3	435	0.1	31.3	4.29				
TY-52	256.2	87.6	5.2	481	0.17	24.9	437	0.2	30.9	3.17				
TY-51	258.6	88.5	4.8	465	0.10	22.4	436	0.2	32.0	3.58				
TY-50	260.4	89.1	4.3	269	0.13	11.6	426	0.1	42.0	16.00				